

**WIDEBAND ELECTROMAGNETIC CHARACTERIZATION OF PORTLAND
CEMENT CONCRETE**

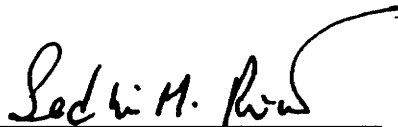
by

Raqibul Mostafa

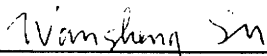
**Thesis submitted to the Faculty of the
Virginia Polytechnic Institute and State University
in partial fulfillment of the requirements for the degree of**

**Masters of Science
in
Electrical Engineering**

APPROVED:



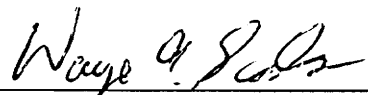
Sedki M. Riad, Chairman



Wansheng Su



Imad L. Al-Qadi



Wayne A. Scales



Aicha Elshabini-Riad

OCTOBER, 1995

LD
5655
V865
1995
M678
c.2

WIDEBAND ELECTROMAGNETIC CHARACTERIZATION OF PORTLAND CEMENT CONCRETE

by

Raqibul Mostafa
Chairman: Dr. Sedki M. Riad
Electrical Engineering

(ABSTRACT)

Wideband electromagnetic characterization of Portland cement concrete (PCC) has been investigated in this study. This is necessary to correlate the material properties of PCC with its physical condition and hence aid in nondestructive evaluation of practical PCC structures. A test fixture has been designed to characterize PCC test specimens in the frequency range of 100-1000 MHz. Measurements have been performed in both time domain and frequency domain. The focus of this research has been to investigate time domain techniques for the characterization of PCC specimens under different test conditions. A simplified TDR measurement technique using one-port calibration scheme has been proposed for the research. Measurements have been carried on reference materials (e.g. Teflon) to verify the accuracy of the proposed technique. Extensive calibration and de-embedding have been studied to minimize the systematic errors involved in the measurement process. A computer simulation based verification process has been studied to validate the proposed calibration and de-embedding scheme. Sensitivity analysis and study of repeatability of the measurement process has been done as well.

ACKNOWLEDGMENT

I would like to express my profound gratitude to Dr. Sedki M. Riad to provide me with an opportunity to do research in the field of time domain measurements and for his fatherly guidance, encouragement and support during my entire research period. I am greatly indebted to him for his valuable advice which made the whole research a reality and a fruitful one.

I would also like to express my appreciation to the committee members, Aicha Elshabini-Riad, Imad L. Al-Qadi, Wansheng Su, Wayne A. Scales for their suggestions and advice along the way. This helped me in looking at the problems from different perspectives and thus enhancing the quality of the study.

I would like to thank my parents and my brother for their care and support which helped me reach where I am. Thanks also goes to my friends Iman and Ahmed, David and Dawn, Tanya and Musa for their whole hearted help when I needed it.

I would like to acknowledge National Science Foundation (NSF) for supporting this research.

TABLE OF CONTENTS

CHAPTER 1: INTRODUCTION

| | |
|---------------------------------------|---|
| 1.0 Introduction..... | 1 |
| 1.1 Frequency Domain Measurement..... | 4 |
| 1.2 Time Domain Measurement..... | 4 |
| 1.3 Non-destructive Testing..... | 6 |
| 1.4 Organization of the Thesis..... | 9 |

CHAPTER 2: DESIGN OF A COAXIAL FIXTURE

| | |
|---|----|
| 2.0 Introduction..... | 12 |
| 2.1 Coaxial Transmission Line..... | 13 |
| 2.1.1 Distributed Resistance, R | 15 |
| 2.1.2 Distributed Inductance, L | 16 |
| 2.1.3 Distributed Capacitance, C | 16 |
| 2.1.4 Distributed Conductance, G | 17 |
| 2.2 Propagation Characteristics..... | 18 |
| 2.2.1 Propagation Constant, γ | 18 |
| 2.2.2 Characteristic Impedance, Z_0 | 19 |
| 2.3 Mode of Propagation..... | 19 |
| 2.4 Design of the Fixture..... | 20 |
| 2.4.1 Tapered Section..... | 22 |
| 2.4.2 Buffer Section..... | 23 |
| 2.4.3 Specimen Holder..... | 25 |
| 2.4.4 Test Specimen..... | 26 |
| 2.4.5 Fixture Accessories..... | 27 |
| 2.5 Electrical Parameters of the Coaxial Fixture..... | 28 |
| 2.5.1 Distributed Resistance, R | 29 |
| 2.5.2 Distributed Inductance, L | 29 |
| 2.5.3 Distributed Capacitance, C | 30 |
| 2.5.4 Distributed Conductance, G | 30 |
| 2.5.5 Characteristic Impedance, Z_0 | 30 |
| 2.5.6 Propagation Constant, γ | 30 |
| 2.5.8 Mode of Propagation..... | 31 |

CHAPTER 3: MATERIAL CHARACTERIZATION IN FREQUENCY DOMAIN

| | |
|---|----|
| 3.0 Introduction..... | 33 |
| 3.1 Theoretical Background..... | 33 |
| 3.2 Frequency Domain Measurement Setup..... | 37 |
| 3.3 Calibration..... | 37 |
| 3.4 Results..... | 43 |

CHAPTER 4: MATERIAL CHARACTERIZATION IN TIME DOMAIN

4.0 Introduction..... 48
4.1 Time Domain Measurement: An Overview..... 48
4.2 Time Domain Measurement: Concepts..... 51
 4.2.1 Time Domain Reflectometry..... 52
 4.2.2 Time Domain Transmission..... 58
4.3 Material Characterization in Time Domain..... 61
4.4 Fourier Transform..... 65
4.5 Dielectric Spectroscopy with the Fixture..... 67
 4.5.1 Principle..... 67
 4.5.2 Measurement Setup..... 68
 4.5.3 Procedure..... 70
 4.5.4 Results..... 70

CHAPTER 5: TIME DOMAIN CALIBRATION AND DE-EMBEDDING

5.0 Introduction..... 78
5.1 TD calibration for Modeling the Fixture..... 79
5.2 De-embedding Process..... 85
5.3 Verification..... 86
5.4 Sensitivity Analysis..... 89
5.5 Extension of the De-embedding Process..... 91

CHAPTER 6: CONCLUSIONS

6.0 Summary..... 96
6.1 Results and Conclusions..... 97

APPENDIX..... 99

REFERENCES..... 102

CURRICULUM VITAE..... 107

CHAPTER 1
INTRODUCTION

1.0 INTRODUCTION

The subject of material characterization deals with the evaluation of the properties of a material. In the context of electrical engineering, properties of interest which govern the electrical behavior of a material may include conductivity, relative permittivity and permeability. Usually, these properties need to be evaluated over a particular frequency band. To this extent, measurement techniques have been devised based on electromagnetic wave propagation in a medium. These techniques investigate the electromagnetic behavior of the material under test, and hence the material properties can be extracted from the measurement data by the application of a suitable algorithm. Bussey [1] provides a survey of measurement to characterize for magnetic permeability and electric permittivity at RF (radio and microwave frequencies). In such measurements, the material under test is shaped into a standard electromagnetic configuration such as a parallel plate capacitor, coaxial transmission line, waveguide, resonator or a microstrip line. Measurement can be performed in either frequency domain or time domain. In either case, a proper parameter model representative for the material under test needs to be developed and the parameters of the model are evaluated by the measurement process. Necessary theory can be developed to obtain the desired electromagnetic properties from a knowledge of these parameters. This thesis presents a microwave based measurement technique for material characterization of concrete to aid in the assessment of the physical condition of concrete structures. This is a part of an ongoing research undertaken at Virginia Tech to study the electromagnetic properties of PCC leading to nondestructive

evaluation of PCC structures. The approach is to estimate electromagnetic properties of concrete under different known test conditions. The goal is to come up with a reference database where the properties will be listed for different conditions of concrete and which will be used to compare the measured field data to predict the internal condition of the practical structures. With this view, PCC was characterized in the frequency band of 100 KHz- 10 GHz. The total spectrum was divided into three bands and different test fixtures were used for different bands as described below:

| <i>Frequency Band</i> | <i>Test Fixture</i> |
|-----------------------|---------------------------|
| 100 KHz - 40 MHz | Parallel plate capacitor |
| 100 MHz - 1 GHz | Coaxial transmission line |
| 1 - 10 GHz | TEM horn antenna |

The work presented in this thesis involves characterization of concrete specimens which contain aggregate of maximum size of 1 inch. This way, the specimens emulate the concrete used in the structures and the evaluated electromagnetic properties of such specimens will be representative of the properties of a practical concrete structure. For characterization purpose, a large coaxial fixture has been designed and both time domain and frequency domain measurements have been performed. The main focus here is the investigation into the electromagnetic properties by time domain techniques. Elaborate calibration and de-embedding schemes have been investigated in time domain. This introductory chapter is intended to present a brief review of the microwave measurement techniques and the organization of the thesis. Sections 1.1 and 1.2 discuss the frequency

domain and time domain techniques, respectively. Section 1.3 discusses the non-destructive testing (NDT) concepts and its role in assessing internal deterioration in concrete structures. Section 1.4 presents the organization of the thesis.

1.1 FREQUENCY DOMAIN MEASUREMENT

Frequency domain measurement implies continuous wave (CW) operation where frequency sweep is used to cover the bandwidth of interest. A measurement set up in this case would include a vector network analyzer (VNA), connecting cables and the electromagnetic configuration to contain the test specimen. Depending upon the set up at hand, a one port or a two port measurement technique can be used. Extensive calibration scheme needs to be employed to ensure accuracy in such measurements.

1.2 TIME DOMAIN MEASUREMENT

In time domain (TD) measurement, the temporal behavior of a material is investigated with an impulse or a step signal acting as the input. As in frequency domain measurement, the end results are the frequency dependent scattering parameters of the test material. In this case, a duration limited incident and reflected and/or transmitted waveforms are acquired and subsequently processed to yield the desired material properties. The special feature of time domain measurement technique is that broadband characterization can be covered in a single measurement and calibration schemes are simpler. The choice of a frequency domain or time domain technique rests on the dielectric

behavior or relaxation time of the material [2]. A long relaxation time implies small bandwidth and frequency sweep technique using VNA is more appealing as a small number of frequency points are needed to cover the required bandwidth. On the other hand, a short relaxation time implies a large bandwidth, for which, time domain technique would be the proper choice. A typical time domain measurement set up would include digital sampling oscilloscope, pulse generator and transmission lines to contain the test material, computer interface and a computer.

Time domain reflectometry (TDR) techniques have been used for signature analysis in ground penetration radar (GPR) and location of faults in telephone cables. Nicolson [3] provides a TD technique to evaluate the relative permittivity, ϵ_r and the relative permeability, μ_r of a test specimen placed in a transmission line. Fellner- Feldegg [4]-[6] provides the use of TD spectroscopy techniques to study the permittivity and relaxation time of polar liquids. Cole [7] presents a TD method to evaluate ϵ_r of a dielectric used as a termination in a transmission line. Sharaawi discusses extension of Cole's method to perform TD spectroscopy of layered dielectric material [8]. Fidanboyu [9], [10] discusses TD approach to characterize material using stripline geometry. Here, a lossy transmission line model is sought for the stripline and an iterative solution for ϵ_r is found based on the comparison of simulated and experimentally obtained TD waveforms.

1.3 NON-DESTRUCTIVE TESTING (NDT)

Non-destructive testing (NDT) is one branch of testing of material properties which is non-invasive in nature and does not disturb the test material during the measurement process. One typical example can be testing of a rail track for identification and location of possible cracks. The non-destructive testing is an attractive feature in the assessment of the existing building structures. Preservation through maintenance and rehabilitation activities is the current approach in the field of civil engineering infrastructure [11]. This requires that the facilities performance be assessed on a regular basis and such assessment can rely on either destructive or non-destructive testing. The factors that dictate the choice include the type of measurements, the required accuracy, the time available, the cost and on the availability of the proper technology. NDT techniques are usually quicker, covers larger area. These advantages of NDT techniques have brought promise in the field of quantitative assessment of concrete structures. Millions of dollars are spent each year in the United States to repair deteriorated concrete structures, mainly due to freeze-thaw damage, reinforcing steel corrosion, and aggregate/matrix separation caused by chemical reactions. For the most parts, these mechanisms are active under the surface, and can not be accurately assessed by visual observation. Therefore, much of the repair and rehabilitation funds are spent to fix conditions that are not seen until the work is contracted and the repair begins or until the deterioration is visible and thus has reached an advanced stage which may jeopardize the structural stability of the facility.

The book by Mehta [12] provides on the components of modern concrete. Some definitions from that book regarding concrete are introduced in this work. Concrete is a composite mixture consisting of binding material and fragments of aggregates embedded in the binding paste. The aggregate is referred to as the granular material, which can include sand, gravel, crushed stone and iron-blast furnace slag. There are two types of aggregates, namely, coarse aggregate (aggregates larger than 4.75 mm) and fine aggregates (aggregates smaller than 4.75 mm but larger than 75 μm). Mortar is formed from a mixture of sand, cement and water and is devoid of coarse aggregates. Cement basically consists of finely pulverized material and provides binding property from hydration process resulting from mixing cement with water. Portland cement is the most commonly used cement and consists mostly of calcium silicates. The hydration processes are stable in aqueous environment.

During the hydration process of cement, the concrete structure undergoes internal changes [13]. Capillary pores and gel pores are formed during the process. Distribution of water also undergoes changes. Water is held in cement in the following ways

- water combined with hydrated cement,
- absorbed water held by surface forces of gel particles,
- water contained in the capillary and gel pores.

Capillary water can be classified into free water (void size > 50 nm) and the water contained in voids (size < 50 nm) [12]. The presence of water greatly dictates the loss component or the imaginary part of ϵ_r .

Portland cement concrete (PCC) is a composite material that contains a wide variety of materials that have different electrical properties. Electrical characterization of concrete can be utilized to reveal information about its mechanical response properties. The electrical properties of interest in this regard are conductivity and relative permittivity (dielectric constant). These electrical properties are related to the composite properties of the aggregates, aggregate size, cast w/c ratio, chloride and moisture content, and reinforcing steel. The deterioration of PCC often results in changes in its electromagnetic properties. These changes occur due to changes in the microscopic structure of the material, such as additional interfaces in dielectric discontinuities created by cracks caused by corrosion, alkali-silica reaction, and/or freeze-thaw damage. Thus, a continuous monitoring of the electromagnetic properties of the structures can indicate to the possibility of any internal changes.

Characterization of PCC over low RF band has been done by Al-Qadi *et. al.* [14]. A parallel plate capacitor fixture is used to contain the concrete specimen and an impedance measurement is done on the fixture, assuming a lumped capacitor model for the specimen. Characterization with coaxial transmission line method has been reported in [11], [15]. Low frequency electrical characteristics of fresh concrete is reported by Whittington [13], where a low resistivity model is assumed for the concrete specimen. A parallel plate transmission line along with impedance measurement is used in [16] to study the electrical properties of concrete as a function of frequency. Chew [17] presents dielectric characterization using a large broadband cell based on a coaxial line geometry.

1.4 ORGANIZATION OF THE THESIS

From the discussion on concrete in the previous section, it is seen that concrete is an inhomogeneous mixture resulting from mixtures of different components and the internal structure consisting of a random distribution of different pores. Thus to characterize concrete, one needs a relatively large volume of specimen so that the random spatial distributions cancel out and an overall average picture about the material properties can be obtained. This chapter has so far reviewed the concepts of frequency domain and time domain measurement techniques and the research in material characterization. The layout of the work done in the characterization process is given below.

Chapter 2 focuses on the design of a coaxial fixture. The chapter begins by reviewing electrical parameters and basic propagation characteristics of a coaxial transmission line. Then, the design of a coaxial fixture for material characterization is discussed. This includes discussion on different sections of the fixture and its associated parameters.

Chapter 3 discusses frequency domain measurement techniques using the coaxial fixture. The chapter starts with theoretical background to evaluate both ϵ_r and μ_r . The experimental set up used in the measurement is discussed next. It then discusses frequency domain calibration process involved in the measurement. It provides an overview of the principle of calibration process and the type used in this measurement method. This is followed by presentation of the results.

Chapter 4 deals with dielectric spectroscopy in time domain. The chapter starts with an overview of the TD measurement principles and concepts. Next, the chapter discusses TDR and TDT techniques with illustrations. Then, it focuses on material characterization in TD. Different methodologies in this field are reviewed and the computation of FFT for TDR waveforms are discussed. The experimental set up used in this research is discussed followed by discussions on results.

Chapter 5 deals with modeling of the coaxial fixture with a scattering parameter network. This is done by TD calibration techniques. Then, a de-embedding process is discussed whereby the ϵ_r of a test specimen is derived from numerical solution of a transcendental equation. Then, an extension of the de-embedding process is discussed where the permittivity plots obtained from the simplified one port measurement is corrected.

Chapter 6 summarizes the work done in this regard and draws general conclusions about the results obtained.

CHAPTER 2
DESIGN OF A COAXIAL FIXTURE

2.0 INTRODUCTION

In this chapter, the design aspects of a measurement device to measure the permittivity and permeability of concrete are discussed. There are several possible candidates for the electromagnetic configuration of the test fixture. The intended frequency range of measurement is 100 - 1000 MHz. The candidates include parallel plate capacitor, coaxial transmission line, cavity resonators and open space radiation systems. Parallel plate capacitor configuration has already been applied in the low RF range in another part of the current research. Rectangular waveguides are not chosen due to the bandwidth limitation of the single mode operating region. Resonator cavities are based on the measurement of resonant frequency and Q of the cavity and implies frequency domain operation. Open space radiation systems commonly employ antenna configurations. For the frequency range of interest, it is difficult to design an antenna to operate at that low frequency range with an efficient beamwidth and a good radiation pattern. In view of the preceding discussions, a coaxial transmission line configuration is chosen as the test fixture. Theory on wave propagation in coaxial line in the presence of test specimen is discussed in details in [42]. The mechanism of generation of evanescent modes and their effects are important in such material characterization technique and is also covered in the same reference. The coaxial fixture is designed to provide reliable and accurate operation both in frequency domain and time domain measurements. Discussion on the physical dimensions and different characteristic parameters is presented.

2.1 COAXIAL TRANSMISSION LINE

Transmission lines are very important for signal propagation and transmission of energy between a source and a load. Among different varieties of transmission lines, coaxial lines are used in numerous applications. The popularity stems from the advantages a coaxial transmission line offers: simple configuration, ease of manufacture and maintenance, wide frequency range and reliable operation. The applications include use as connecting cables between instruments and use in microwave devices. Quality of a transmission line depends upon its ability to transmit signals with as low loss as possible. This in turn depends on the electrical parameters of the line. The geometry and dimension of a transmission line will indicate the possible modes of energy propagation. Complete treatment of these aspects of transmission lines with respect to coaxial lines can be found in most books on electromagnetics. In this section, a brief discussion on the characteristics of a coaxial transmission line and the design of a coaxial fixture will be presented.

A coaxial transmission basically consists of two concentric, cylindrical conductors. The inner or center conductor can be hollow or solid. The gap between the center and outer conductor can contain air or it can be filled with any dielectric material. In such a configuration, the electromagnetic fields are confined inside as they propagate along the line. Figure 2.1 shows a schematic of a coaxial line.

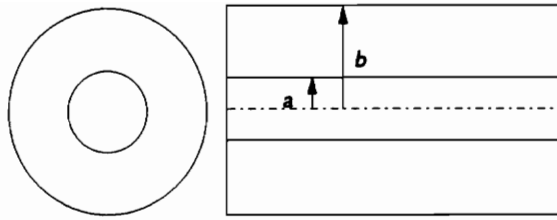


Figure 2.1 Schematic of a coaxial transmission line.

For analysis purpose, a transmission line is often modeled as an electrical network of distributed passive elements. A coaxial transmission line can be characterized by four electrical properties, namely;

- a distributed resistance
- a distributed inductance
- a distributed capacitance
- a distributed conductance

These properties in turn determine the important parameters such as characteristic impedance, propagation constant and velocity of propagation. A complete graphical treatment of these parameters for air-dielectric coaxial lines can be found in the NBS Monograph 96 [18]. It covers precision coaxial lines where the size varies from 7 mm to 21 mm. For a more general discussion, one can refer to the books by Chipman [19], Ramo and Whinnery [20].

2.1.1 Distributed resistance, R :

This parameter incorporates the total series resistance per unit length of the conductors constituting the transmission line. This parameter is dependent upon the material used, the radii of the conductors and the frequency of operation. It is treated as an internal quantity being independent of the nature of the dielectric filling the interconductor space. For a particular coaxial line, the resistance increases over the d.c. value with increasing frequency due to the skin effect. The current in this case tends to flow in a shallow depth in periphery rather than being uniformly distributed over the conductor. This has led to the technique of using a thin plate of high conductivity on a core metal. At high frequencies, current flow is dependent upon the plating material with negligible effect of the core metal.

If δ represents the skin depth, then for $a/\delta > 100$, and $b/\delta > 100$ and the thickness of the conductors being greater than 3δ , we have the following simplified expression [19]:

$$\text{Inner Conductor: } R = \frac{R_s}{2\pi a} \Omega/\text{m} \quad (2.1a)$$

$$\text{Outer Conductor: } R = \frac{R_s}{2\pi b} \Omega/\text{m} \quad (2.1b)$$

$$\text{Total: } R = \frac{R_s}{2\pi b} \left[1 + \frac{b}{a} \right] \Omega/\text{m} \quad (2.2)$$

where R_s is the surface resistivity as given by

$$R_s = \frac{1}{\sigma\delta} = \sqrt{\frac{\omega\mu}{2\sigma}} \Omega \quad (2.3)$$

where, σ =conductivity of the metal used,

$\omega = 2\pi f$, angular frequency,

μ = permeability of the metal used.

2.1.2 *Distributed Inductance, L:*

This represents the total series inductance arising from the effect of magnetic field due to the current in both inner and outer conductors. The magnetic field lies in both the inner conductor and in the dielectric space and thus L contains both internal and external component. At high frequencies, in megahertz and above, most of the current rises to the surface leaving virtually very small current around the center and this leads to a small amount of flux linkage in the conductor and hence a very small value for the internal inductance. The total inductance at high frequencies is thus governed by the external component. At low frequencies, the internal component can not be assumed negligible and has to be considered in the calculation of total inductance.

For nonmagnetic dielectric, which is usually the case, the external inductance is independent of frequency. The expression for external inductance L_x can be written as

[19]

$$L_x = \frac{\mu}{2\pi} \ln \frac{b}{a} \text{ henry/m.} \quad (2.4)$$

2.1.3 *Distributed Capacitance, C:*

This parameter represents the total shunt capacitance between the conductors per unit length. It is an external quantity in that it depends on the type and dimensions of dielectric medium. The material or the thickness of the conductors does not affect this parameter. The nature of the distribution of electric field in the dielectric medium is the factor concerning the distributed capacitor. The interconductor space is usually filled with

low loss material having low dielectric constant. It can be also be a lossy material with high values of dielectric constant as in the case of material testing. Usual dielectric materials include Teflon, polyethylene and steatic ceramics.

The expression for C is given by

$$C = \frac{2\pi\epsilon'}{\ln(b/a)} \text{ farads/m} \quad (2.5)$$

where, ϵ' = real part of the permitivitty of the dielectric material.

In general, distributed capacitance is very stable over a wide frequency range since the dielectric materials commonly used show at most several percent variations over a wide frequency range (typically 60 Hz to 10 GHz).

2.1.4 *Distributed Conductance, G:*

This is a representation of the total shunt conductance per unit length. Conductance, in the usual sense, is related to the phenomenon of any charge carrying particles. If the dielectric material allows flow of charge carriers, then a value of conductivity can be assigned to the transmission line, from the concept of resistance. But in most cases, such a value of conductance arises from dielectric losses such as polarization losses. The material though lossy, remains nonconductive at d.c. signals. These losses are incorporated of the material by assigning complex number to the material permitivitty. The permitivitty in this case can be written as

$$\epsilon = \epsilon' - j\epsilon'' \quad (2.6)$$

Using the concept of admittance, this leads to the following expression for conductance

$$G = \omega \frac{\epsilon''}{\epsilon'} \frac{2\pi\epsilon'}{\ln(b/a)} = \omega C \tan \delta \text{ mho/m} \quad (2.7)$$

where δ is the angle between ϵ' and ϵ'' expressed as $\tan\delta = \epsilon''/\epsilon'$, and $\tan\delta$ is often termed as the loss tangent.

In the commonly used coaxial lines with low loss dielectric materials, the value of conductance is too small to be perceivable. The loss tangent, for example, in the case of polyethylene is .0002 in the frequency range (Hz-GHz).

2.2 PROPAGATION CHARACTERISTICS

The electrical parameters discussed above can be used to determine the propagation characteristics of a coaxial line. The characteristics of interest in this case are:

- propagation constant, γ ;
- characteristic impedance, Z_o ;

2.2.1 Propagation constant, γ

It indicates the attenuation and phase shift of the line offered to the propagating signal by a transmission line. The expression for γ is

$$\gamma = \alpha + j\beta = \sqrt{(R + j\omega L)(G + j\omega C)} \quad (2.8)$$

where, α = attenuation constant,

β = phase constant.

For high-frequency applications where $R/\omega L \ll 1$ and $G/\omega C \ll 1$, the expression can be approximated as

$$\gamma \cong j\omega \sqrt{LC} \quad (2.9)$$

2.2.2 Characteristic impedance, Z_o

It is the impedance seen by an input signal into a transmission line. The expression for Z_o is

$$Z_o = R_o + jX_o = \sqrt{\frac{R + j\omega L}{G + j\omega C}} \quad (2.10)$$

Using the high-frequency approximation, Z_o can be written as

$$Z_o \cong \sqrt{\frac{L}{C}} \quad (2.11)$$

2.3 MODE OF PROPAGATION:

The principal mode of energy propagation in a coaxial line is the transverse electromagnetic (TEM) mode. In this mode, the electric field is radial and the magnetic field is circular and concentric with the conductors and both the fields lie in the transverse plane. But under certain conditions, higher order modes can be excited in a coaxial line and these modes can contribute to wave propagation. For TE and TM waves supported by these higher order modes, there is a cut-off value of wave number below which the modes can not be sustained. The cut-off condition can be determined by solving

transcendental equations containing Bessel functions [20]. The cut-off wave number is a function of the radii of the conductors. The cut-off condition can be written as

$$f_c = \frac{k_c}{2\pi\sqrt{\mu_1\varepsilon_1}} \quad (2.12)$$

where, f_c = cut-off frequency.

k_c = cut-off wave number.

μ_1 = permeability of dielectric material.

ε_1 = permittivity of dielectric material.

Graphical methods can be used in the case of TM modes for determining the cut-off wavelength for particular values of the radii a and b . Approximate formulas are available when the radius of curvature of the conductors is relatively large. The two dimensions that govern the cut-off condition are interconductor distance ($b-a$) and the average circumference, $(a+b)/2$. The analogous situation is the rectangular waveguide and thus the cut-off condition is dictated by the number of half wavelengths the two dimensions can accommodate. The approximate cut-off condition is given as [20]

$$\lambda_c \cong \frac{2}{p}(b-a) \quad \text{TM} \quad (2.13a)$$

$$\lambda_c \cong \frac{2\pi(b+a)}{n \cdot 2} \quad \text{TE} \quad (2.13b)$$

2.4 DESIGN OF THE FIXTURE:

The coaxial fixture is designed with dimensions that can contain large concrete specimens. This is in order to test specimens that can accommodate aggregates commonly used in practice. The dimensions of the fixture are quite different from coaxial lines

commonly employed in signal transmission or in testing purpose. The principal mode of propagation is the TEM mode. The material used for the conductors is brass.

The coaxial fixture is a symmetrical device in design and comprises of the following sections:

- Two pieces of Tapered Section.
- Two pieces of Buffer Section.
- One piece of Specimen Holder.

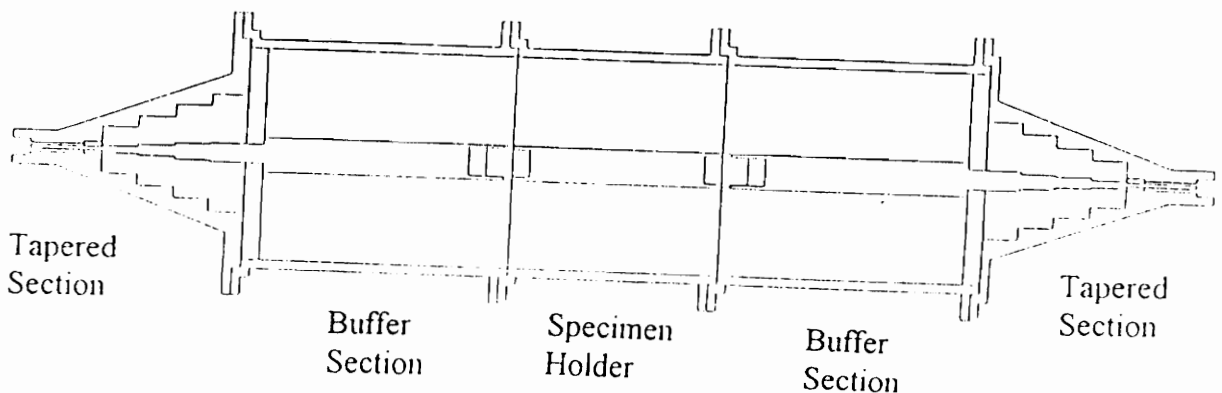


Figure 2.2 Cross sectional view of the coaxial fixture.

The fixture begins at one end with the tapered section. This section combines with the buffer section to form one end for input signal. The buffer or isolation section is followed by the specimen holder. The other side of the fixture is symmetrical about the specimen holder. The whole fixture when assembled takes the form of a large cylindrical object with two conical ends. Figure 2.2 illustrates the complete fixture. A brief description of each component is presented in the following sub-sections.

2.4.1 *Tapered Section:*

At one end, the designed coaxial tapered section houses an APC 7 connector to connect the test measurement cable to the fixture. This end is designed to be $50\ \Omega$ to match the instruments and connecting cables. The coaxial dimensions at the other end of the tapered section is designed to match the dimensions of the fixture. This results in a $100\ \Omega$ characteristic impedance for the air section of the coaxial line in the vicinity of the material under test. Thus the tapered section provides a transition from $50\ \Omega$ to the $100\ \Omega$. To minimize mismatch in the transition zone, both the inner and outer conductors must undergo dimension change in gradual fashion. Due to difficulties in the manufacturing process to provide gradual change, several small steps were incorporated in the inner and outer conductor dimensions; there are four steps in total. The presence of step discontinuities can generate local waves at the discontinuities which can affect measurements both in time domain and frequency domain [43]. If the impedance transition occurs in one step, large discontinuity is presented to the propagating signals, resulting in a gross distortion of field distributions and generation of higher order modes. The design of several small steps instead of one large step is thus preferred to reduce the amount of reflections at the discontinuities. This is specifically true in the case of time domain measurement where a large reflection from a discontinuity can perturb the required reflection from the test specimen and mask the necessary information all together. Figure 2.3 illustrates a sectional view of this section with the dimensions included. The inner conductor runs along the whole length of the buffer section as well.

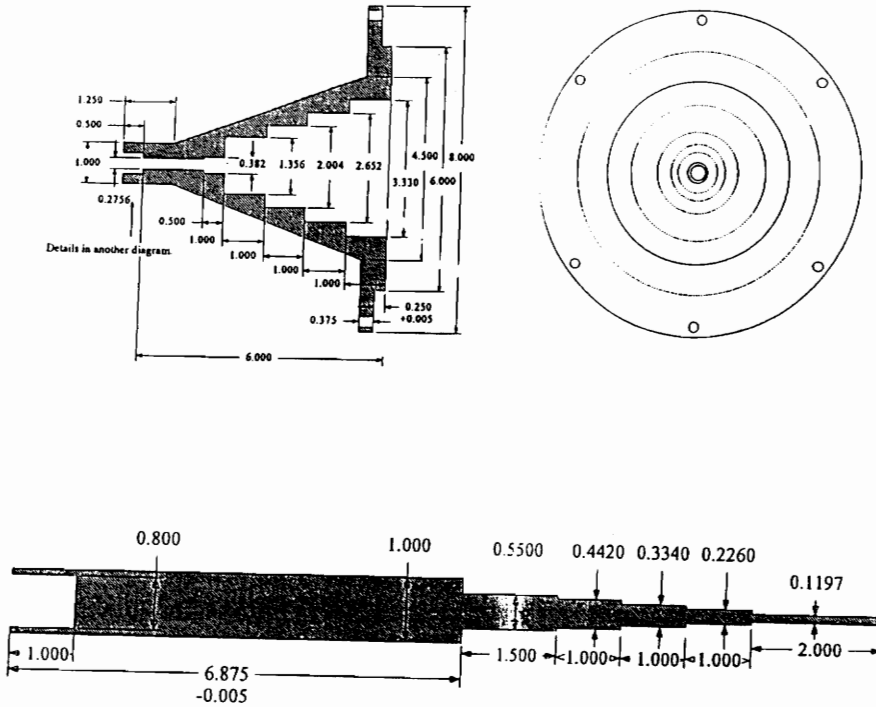


Figure 2.3 Sectional view of the tapered section with center conductor. (Dimensions in inch)

2.4.2 Buffer Section:

This is a cylindrical section which assumes the same dimensions as the specimen holder. Thus a truly coaxial transmission line begins from this section. At one end, it mates with the tapered section and the two are secured by bolting them together. At this junction, the buffer section contains a circular Teflon washer which supports the center conductor. At the other end, the buffer section connects to the specimen holder section. The inner diameter of the outer conductor ($2b$) is 15 cm (~ 6 inch) and the outer diameter

of the inner conductor ($2a$) is 2.54 cm (1 inch). This results in a characteristic impedance different from 50Ω . If the impedance is to be maintained at 50Ω , the dimensions become excessively large in order to accommodate large aggregates. The dielectric medium is air. The length of this section is 15 cm (6 inch). In time domain measurements, this section provides a time delay between the reflected signals from the tapered section and the test specimen, otherwise overlapping of these signals will destroy the information about the specimen. Assuming air-dielectric, the time for round trip for signals within this section is

$$t \approx \frac{2l}{c} \approx \frac{30}{3 \times 10^{10}} = 1 \text{ ns.}$$

where l is the length of the section in cm and c is the velocity of light (free space) in cm/sec.

Thus it will provide a time delay of 1 ns between signals reflected from the tapered section and the front face of the specimen. This will indicate the size and position of time epoch required in time domain measurements. The buffer section can also serve to damp the local waves generated at the step discontinuities in the tapered section. The inner conductor of the tapered section continues through out the length of this section. Figure 2.4 illustrates the cross sectional view of the buffer section.

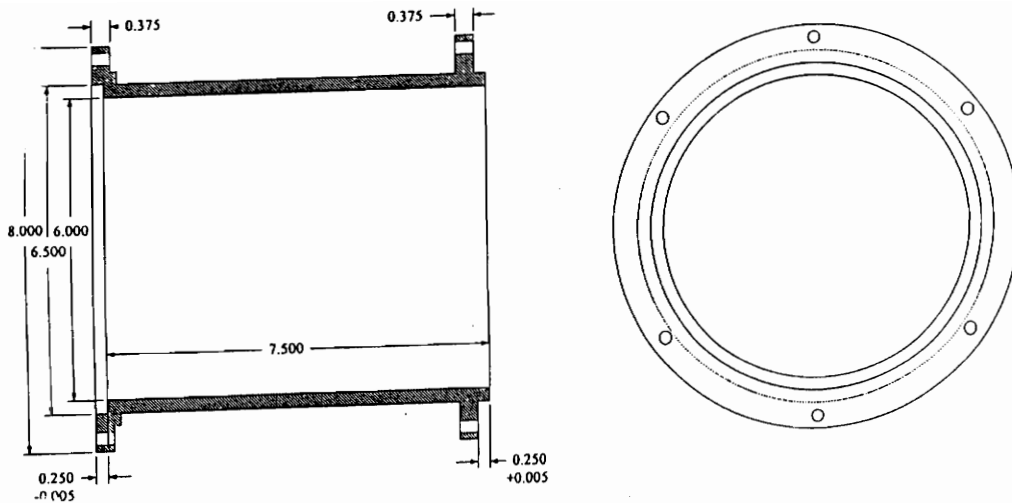


Figure 2.4 Sectional view of buffer section. (Dimensions in inch)

2.4.3 Specimen Holder:

This component of the fixture contains the test specimen. The outer conductor is split into two halves to allow for easy insertion and removal of concrete specimens. The cylindrical test specimen is first placed on the bottom half and the top half is put on the specimen to contain the specimen completely. This kind of arrangement offers the advantages of protection of the inner surface during insertion/removal against friction and abrasion, close contact of the conductors and the specimen and thus minimum air gap and reliability and ease of operation. A cylindrical brass rod inside the test specimen provides the center conductor. This section is bolted to the buffer section to provide a firm connection between the two. The diameters and the length of the conductors are the same as in the buffer section. The length will provide a time delay of 1 ns between the reflected

signals from the two faces of the test specimen. This information is necessary when time domain measurements are involved. Figure 2.5 shows the sectional view of the specimen holder.

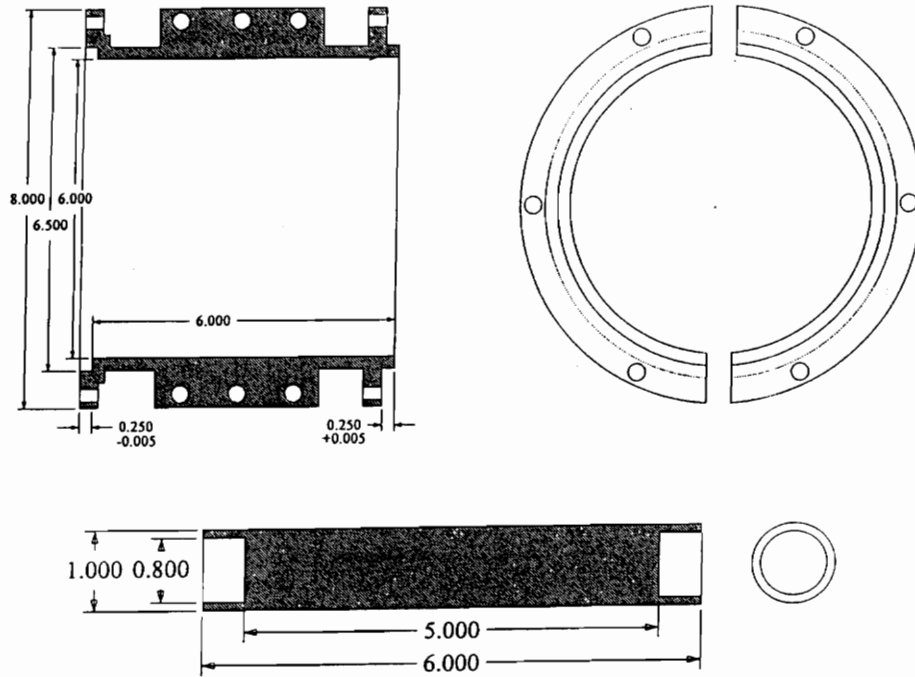


Figure 2.5 Sectional view of specimen holder and center conductor. (Dimensions in inch)

2.4.4 Test Specimen

The test specimen is a cylindrical concrete specimen. The specimen is designed to accommodate aggregates which are typically used in the concrete structures. This will allow the measurement set-up to generate data which will be representative of real life concrete structures for all practical purposes. The surfaces of both the end faces are given a smooth finish to provide uniform reflection. The curved surface is cast in a mold to

give a smooth finish but sometimes non-uniformity is unavoidable because of falling out of loose aggregates. The specimens are cast with cylindrical brass rods at the center to act as center conductors in the specimen holder. The dimensions of interest are

outer diameter of the specimen: 15 cm (6 inch).

outer diameter of the center conductor: 2.54 cm (1 inch).

length of the specimen: 15 cm (6 inch).

These dimensions allow for maximum aggregate of size of 2.54 cm (1 inch) in the specimen which are practically used.

The preparation of a concrete specimen begins with mixing cement with aggregate in a mixer. Then the mix is put into a cylindrical mold of proper dimension. The center conductor is screwed to the bottom plate of the mold. The frame of the mold can be adjusted in the form of a clamp and this provides a smooth uniform cylindrical surface for the specimen. The cast specimen is removed from the mold one day after casting and put into a curing room for subsequent measurement.

2.4.5 Fixture Accessories

Among accessories, there are small solid cylindrical connectors and a solid circular brass plate. The connectors are made from brass and are used to connect the center conductors of different sections. They are designed to provide a continuous connection without any air gap which may result from a slack in the conductors. The circular brass plate is designed to mate to buffer section. The plate provides the reflection standard in

frequency domain calibration and reference waveform in time domain measurements. In context of electrical network , this provides a highly reflective termination to the test signals and acts as a "short circuit". Figure 2.6 shows schematic of connector and the brass plate.

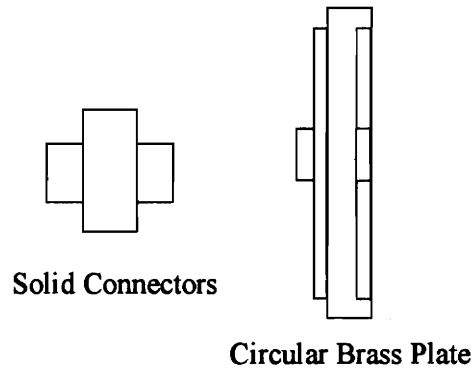


Figure 2.6 Solid connector and metallic plate (side view).

2.5 ELECTRICAL PARAMETERS OF THE COAXIAL FIXTURE:

The transmission line parameters discussed in a previous section will be evaluated for the designed fixture. Discussion will be limited to actual coaxial line sections, i.e. buffer or specimen holder. The tapered section due to its conical shape will not be included for discussion.

The physical parameters of the coaxial line are

Outer radius of inner conductor, $a = 1.27$ cm (0.5 inch).

Inner radius of outer conductor, $b = 7.62$ cm (3 inch).

Material: Brass.

Conductivity, $\sigma = 1.57 \times 10^7$ mhos/m.

Permeability, $\mu = 4\pi \times 10^{-7}$ henries/m

Frequency Range: (100-1000) MHz.

2.5.1 Resistance, R :

First the surface resistivity R_s is determined as a function of frequency, f , as

$$R_s = \sqrt{\frac{\pi f \mu}{\sigma}} = 5.01 \times 10^{-7} \sqrt{f} \ \Omega$$

$$\begin{aligned} \text{So, } R_s &= 5.0145 \times 10^{-3} \ \Omega \text{ at } f = 100 \text{ MHz} \\ &= 15.857 \times 10^{-3} \ \Omega \text{ at } f = 1000 \text{ MHz} \end{aligned}$$

Then the distributed resistance R can be determined by the high frequency approximation (equation 2.2)

$$R = \frac{R_s}{2\pi b} \left[1 + \frac{b}{a} \right]$$

With the given values of b , a and R_s , R can be evaluated as

$$\begin{aligned} R &= 7.33 \times 10^{-2} \ \Omega/\text{m} \text{ at } f = 100 \text{ MHz} \\ &= 23.183 \times 10^{-2} \ \Omega/\text{m} \text{ at } f = 1000 \text{ MHz} \end{aligned}$$

2.5.2 Inductance, L :

At the frequencies of interest, the internal inductance will be a negligible part of the total inductance and the external inductance will be assumed to form the total inductance for all practical purposes. In this case, the total distributed inductance can be evaluated by the high frequency approximation (equation 2.4)

$$L = \text{External Inductance, } L_x = \frac{4\pi \times 10^{-7}}{2\pi} \ln 6 = 3.5835 \times 10^{-7} \ \text{H/m}$$

2.5.3 Capacitance, C :

The capacitance will be evaluated for air-dielectric line by use of (equation 2.5) as

$$C = \frac{4\pi \times 10^{-7}}{2\pi} \ln 6$$
$$= 3.1034405 \times 10^{-11} \text{ farads/m}$$

2.5.4 Conductance, G :

For air-dielectric, the loss tangent can be assumed to be very small and the value of conductance can be taken as zero (equation 2.7) for all practical purposes.

$$G = \omega C \tan \delta \cong 0$$

2.5.5 Characteristic Impedance, Z_o :

Characteristic impedance for the designed transmission line can be found by applying equation 2.10

$$Z_o = \sqrt{\frac{R + \omega L}{G + \omega C}}$$

$$R = 7.33 \times 10^{-2} \Omega/\text{m} \text{ and } \omega L = 225.16 \Omega/\text{m} \quad \text{at } f = 100 \text{ MHz.}$$

$$R = 23.183 \times 10^{-2} \Omega/\text{m} \text{ and } \omega L = 2251.579 \Omega/\text{m} \quad \text{at } f = 1000 \text{ MHz.}$$

Since $R \ll \omega L$, over the frequency range of interest and G is negligibly small, we have the following value of Z_o for the line

$$Z_o \cong \sqrt{\frac{L}{C}} = 107.46 \Omega$$

2.5.6 Propagation constant, γ :

The high frequency approximate formula as given in equation 2.9 will be used to determine the value of γ as

$$\begin{aligned}
\gamma &\cong j\omega\sqrt{LC} = j\omega(3.33485 \times 10^{-9}) \text{ rad/m.} \\
&= j 2.0953 \text{ rad/m} \quad \text{at } f = 100 \text{ MHz} \\
&= j 20.953 \text{ rad/m} \quad \text{at } f = 1000 \text{ MHz}
\end{aligned}$$

2.5.7 Mode of propagation:

For the coaxial line, TEM is the dominant mode of wave propagation. Due to the large dimensions of the designed coaxial line, the possibility of excitation of higher order modes and energy propagation by them exists. For the given dimensions, the cut-off condition for lowest order TM waves can be found from graphical solution of boundary conditions [20].

For lowest order TM modes and assuming air line, we have from the graph, for $b/a = 6$

$$\begin{aligned}
\lambda_c &= 2(b-a) \times 1.03 = 13.081 \text{ cm.} \\
f_c &= \frac{1}{\sqrt{\mu_1 \epsilon_1}} \times \frac{1}{\lambda_c} \\
&= \frac{299.863 \times 10^6 \times 10^2}{13.081} \\
&= 2.292 \text{ GHz}
\end{aligned}$$

For lowest order TE waves, equation 2.13b yields

$$\begin{aligned}
\lambda_c &\cong 2\pi \left(\frac{a+b}{2} \right) \quad \text{with } n=1 \text{ for lowest order mode.} \\
&= 27.928 \text{ cm.} \\
f_c &\cong 1.073671 \text{ GHz}
\end{aligned}$$

CHAPTER 3

MATERIAL CHARACTERIZATION IN

FREQUENCY DOMAIN

3.0 INTRODUCTION

The design of a coaxial fixture to characterize concrete specimens has been discussed in the previous chapter. In this chapter, material characterization in frequency domain with the designed fixture is discussed. A network model is assumed for the test specimen and necessary mathematical formulation is developed to evaluate material properties in terms of the network parameters. Then an experimental set up based on microwave insertion measurement technique, is discussed to obtain the desired network parameters of the specimen. Calibration, an inherent part of such measurement is reviewed in some details and the specific type of calibration scheme used in the set up is discussed. Results of experimentally obtained permittivity and permeability of the test specimen are presented next.

3.1 THEORETICAL BACKGROUND

The measurement techniques involved in this research work rely on the principles of microwave measurement. The specimen to be tested is assumed to be placed between two reference or measurement planes in the case of two-port measurement and at one reference plane in one-port measurement. The measurement techniques assume a scattering parameter or S -parameter model for the specimen under test. The four parameters of this model, S_{11} , S_{21} , S_{12} and S_{22} are determined after calibration process by a network analyzer as a function of frequency. Among the four parameters, S_{11} and S_{21} account for reflection from and transmission through the specimen and indicate the

electrical properties of it. Reflection and transmission at a discontinuity is dependent upon the properties of the material providing the discontinuity. The information about electrical properties of a material such as permittivity and permeability are embedded in the S -parameters. Evaluation of the S -parameters can facilitate one subsequently to determine permittivity and permeability of a material.

Formulations

Assume the specimen has a length d , an impedance Z and propagation constant γ_d . Two sides of the specimen are taken as two reference planes. On both sides of the specimen, the adjacent media has characteristic impedance of Z_0 as shown for a coaxial fixture in figure 3.1. The S -parameter model for the specimen is shown in the same figure.

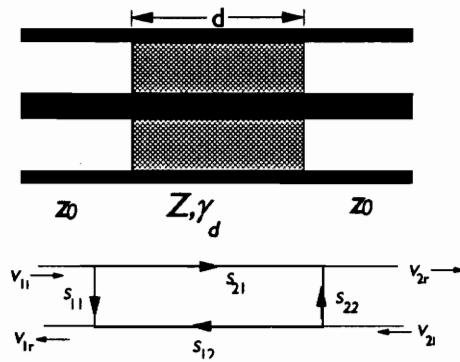


Figure 3.1 Schematic of a specimen in a coaxial line.

The complex reflection co-efficient ρ , of the specimen can be expressed in terms of impedance as follows:

$$\rho = \frac{Z - Z_0}{Z + Z_0} \tag{3.1}$$

In terms of relative permittivity ϵ_r and permeability μ_r , ρ becomes

$$\rho = \frac{\sqrt{\mu_r/\epsilon_r} - 1}{\sqrt{\mu_r/\epsilon_r} + 1} \quad (3.2)$$

A parameter τ , incorporating the propagation constant can be expressed as

$$\tau = e^{-j\omega\sqrt{\mu_r\epsilon_r}\frac{d}{c}} \quad (3.3)$$

where, radian frequency $\omega=2\pi f$, c is the velocity of light in free space and $j = \sqrt{-1}$.

The S -parameters can be related to the reflection coefficient ρ and the term τ .

From [39], the following expressions hold

$$\frac{S_{21}}{1+S_{11}} = \frac{(1+\rho)\tau}{1+\rho\tau^2} \quad (3.4)$$

$$S_{11} = \frac{Z_{in} - Z_0}{Z_{in} + Z_0} = \frac{V_{1r}}{V_{1i}} \quad (3.5)$$

After rearranging terms, the following expressions are obtained for S_{11} and S_{21}

$$S_{11} = \frac{\rho(1 - \tau^2)}{1 - \rho^2\tau^2} \quad (3.6)$$

$$S_{21} = \frac{(1 - \rho^2)\tau}{1 - \rho^2\tau^2} \quad (3.7)$$

The specimen is assumed to be symmetrical, so that $S_{11}=S_{22}$ and $S_{21}=S_{12}$.

From equations 3.6 and 3.7, it can be seen that the ϵ_r and μ_r are contained in ρ and τ and two transcendental equations can be formed whereby ϵ_r and μ_r can be solved iteratively. To overcome this tedious process of solving for ϵ_r and μ_r , the method proposed by Nicolson [3] is followed here. According to [3], one can write,

$$\frac{\mu_r}{\epsilon_r} = \left(\frac{1+\rho}{1-\rho} \right)^2 \quad (3.8)$$

$$\mu_r\epsilon_r = - \left[\frac{c}{\omega d} \ln \left(\frac{1}{\tau} \right) \right]^2 \quad (3.9)$$

The equations above can be solved for ϵ_r and μ_r as

$$\epsilon_r = \frac{1 - \rho j \ln(1/\tau) \cdot c}{1 + \rho} \frac{1}{2\pi f d} \quad (3.10)$$

$$\mu_r = \frac{1 + \rho j \ln(1/\tau) \cdot c}{1 - \rho} \frac{1}{2\pi f d} \quad (3.11)$$

Thus, over a particular range of frequency, a complete set of frequency dependent S_{11} and S_{21} will lead to determination of ϵ_r and μ_r .

3.2 FREQUENCY DOMAIN MEASUREMENT SET-UP

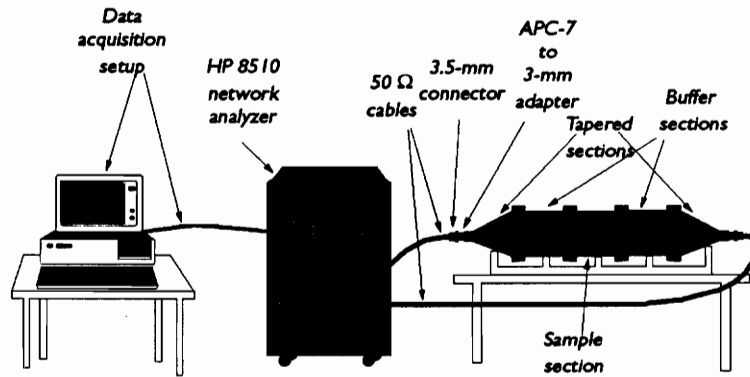


Figure 3.2 Measurement set-up in frequency domain.

The set-up used in measurements is shown in figure 3.2. Here a transmission/reflection (T/R) method based on two port measurement technique is employed. An HP 8510 network analyzer is used for calibration and determining the S -parameters of the concrete specimen. An S -parameter model is assumed for the specimen holder section containing the specimen. Figure 3.3 shows the S -parameter model for the specimen holder along with the complete fixture. After calibration process,

the network analyzer yields the S -parameters of the specimen which can then be processed to obtain the required electrical properties.

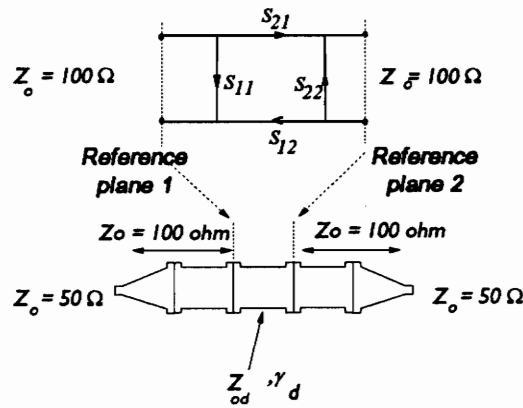


Figure 3.3 S -parameter model for the fixture along with the schematic representation.

3.3 CALIBRATION

In frequency domain measurement, the measuring instrument needs to be calibrated before being used in actual measurement. This is in order to establish a reference plane for microwave insertion measurements. In such measurements, the device under test (DUT) is inserted between the intervening networks (like connecting cables) connecting to the measuring instrument. This technique of measurement is known as two-port measurement and in this case two-port calibration is done at the ends of the intervening networks forming the reference planes, to make measurements free of any effect the connection configuration might have. Sometimes the DUT may be connected to only one channel of the automatic network analyzer and one-port measurement is done to

yield the device characteristics. In such a case, one-port calibration is required. The calibration process aims at standardizing the measurement set-up prior to actual measurement by eliminating possible sources of errors related to the measurement process.

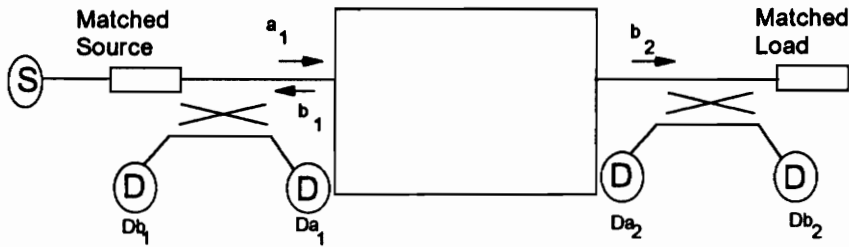


Figure 3.4 Schematic of measurement process in frequency domain.

To exemplify the purpose of calibration, a schematic of two-port measurement model as shown in figure 3.4 will be discussed. Figure 3.4 presents an arbitrary test device inserted between two channels of a network analyzer. In this simplistic model the network analyzer is comprised of directional couplers, signal source and detectors. The measurement model assumes matched terminations at both the load and source sides. Assuming a symmetrical device, measurements of S_{11} and S_{21} will suffice to characterize the device completely. The directional couplers separate the necessary signals into the respective detectors and the received/recorded signal at the detectors provide the information necessary to evaluate S_{11} and S_{21} .

Under the assumption of an ideal error-free condition, the S parameters can be evaluated as

$$S_{11} = \frac{D_{b1}}{D_{a1}} \quad (3.12a)$$

$$S_{21} = \frac{D_{b2}}{D_{a1}} \quad (3.12b)$$

where the D_b and D_a s are detected signals as shown in figure 3.4.

But such a simplistic model does not hold in the presence of errors because the acquired signals become contaminated with the different errors. Possible sources of errors in such a set-up can be:

- Imperfect Connectors
- Lossy Cables.
- Noisy detectors.

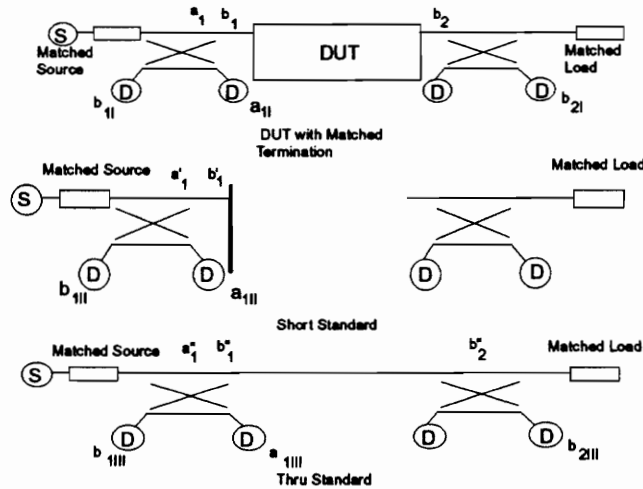


Figure 3.5 Schematic of calibration process.

In the presence of errors or extraneous effects of the different measurement components, one has to resort to the process of calibration. Calibration is done by replacing the DUT with standard terminations of known reflection and transmission properties. There are several possible choices of combination of standard terminations

and the choice of a particular calibration scheme depends upon the bandwidth of interest and the realization of a standard termination in a measurement set up. One such scheme, based on short reference or reflection standard, thru and matched or load termination, is shown in figure 3.5. In this figure, different calibration standards along with the signals at the detectors are shown. Based on the schematic representation in figure 3.5, the computation of the S -parameters, namely S_{11} and S_{21} , in terms of the recorded signals is presented below.

Formulation

From figure 3.5 (matched) , we can write,

$$a_{1I} = C_1 a_1 \quad (3.13a)$$

$$b_{2I} = C_2 b_2 \quad (3.13b)$$

$$b_{1I} = C_3 b_1 \quad (3.13c)$$

where all the errors associated in the measurement process are lumped in the constants C_s .

From figure 3.5 (short), we have,

$$a_{1II} = C_1 a_1' \quad (3.14a)$$

$$b_{1II} = C_3 b_1' \quad (3.14b)$$

$$b_1' = (-1) a_1' \text{ (reflection coefficient} = -1 \text{)}. \quad (3.14c)$$

From figure 3.5 (thru), we have,

$$a_{1III} = C_1 a_1'' \quad (3.15a)$$

$$b_{2III} = C_2 b_2'' \quad (3.15b)$$

$$b_{1III} = C_3 b_1'' \quad (3.15c)$$

$$b_2'' = a_1'' \quad (3.15d)$$

The group of equations from 3.13 to 3.15 can be arranged to come up with the following expressions relating the constants C s to the measured signals,

$$\frac{C_1}{C_3} = -\frac{a_{1II}}{b_{1II}} \quad (3.16a)$$

$$\frac{C_2}{C_3} = \frac{b_{2III}}{a_{1III}} \times \frac{C_1}{C_3} \quad (3.16b)$$

When the device under test is inserted between the measurement planes, the parameters S_{11} and S_{21} can be expressed in terms of the recorded waveforms as

$$S_{11} = \frac{b_{1I}}{a_{1I}} \times \left(-\frac{a_{1II}}{b_{1II}} \right) \quad (3.17a)$$

$$S_{21} = \frac{b_{2I}}{a_{1I}} \times \frac{b_{2III}}{a_{1III}} \times \left(-\frac{a_{1III}}{b_{1III}} \right) \quad (3.17b)$$

So three sets of standards provide the required information for evaluation of S_{11} and S_{21} .

The discussion above presents a simplified model with a view to provide an insight into the measurement process and an appreciation of the calibration technique. For a complete model incorporating all the possible sources of errors, one needs to refer to a twelve (12) term error model [24]. Figure 3.6 shows the complete model with the device embedded in a network of all the possible errors.

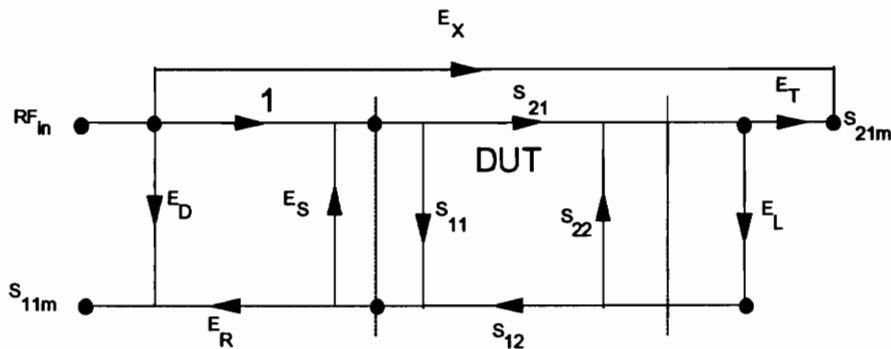


Figure 3.6 Complete error model representation.

The model in figure 3.6 shows six (6) error terms for signal propagation in the forward direction, i.e., from port 1 to port 2. A similar model holds for signal propagation in the reverse direction and hence the total number of error terms are twelve (12). The description of the error terms are:

- E_D ≡ Directivity error (from directional coupler).
- E_S ≡ Effective source error (due to mismatch in source).
- E_R ≡ Transmission error.
- E_T ≡ Transmission tracking error (Due to meters to measure b_1, a_1, \dots)
- E_L ≡ Load reflection error.
- E_X ≡ Cross-talk error (coupling between port 1 and port 2).

S_{11m} and S_{21m} are referred to as the measured values of S_{11} and S_{21} of the test device and represent a modified form of the actual values due to the presence of the error terms. Three different sets of calibration standards are required to de-embed S_{11} and S_{21} from the measured data. They are

- open, reflection and load: to account for E_D, E_R and E_S .
- isolation: for E_X .
- thru: for E_L and E_T .

With a complete knowledge of the error terms (both in the forward and in the reverse direction), the S -parameters of the DUT can be determined from the measured values of the respective S -parameters.

In frequency domain measurement, it is very hard to realize a load standard which will provide a matched termination over the whole frequency range of interest. Because of the dimensions of the coaxial fixture, a matched standard could not be realized physically. Thru, Reflection and Line (TRL) method was used for calibration purpose [22]. Thru standard was realized by directly connecting the two buffer sections. A circular brass plate

was placed at the end of the buffer section to provide the Short or Reflection standard. The Line standard was achieved by using an empty specimen holder and this provided the reference impedance for the measurement system. The calibration configurations are shown in figure 3.7. A program [23] was used to perform the calibration and provided corrected measured data.

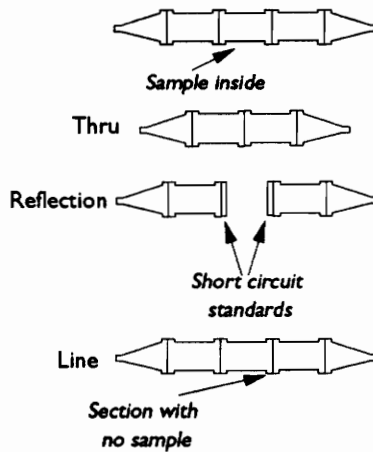


Figure 3.7 Schematic of calibration process.

3.4 RESULTS

A concrete specimen was characterized in frequency domain by the techniques mentioned in the previous sections. The specimen used here was cast using type I Portland cement. The aggregate used was limestone with a maximum aggregate size of 1 inch. The water-to-cement ratio was 0.35 and air entrainment was approximately 3%. The bandwidth of interest was from 50-1000 MHz. Plots for relative permittivity and permeability are shown in figures 3.8 and 3.9, respectively. The dielectric constant starts

from a value of 20 and rolls off and settles down around 11 in the high frequency range. The imaginary part of ϵ_r , or loss component, starts from a high value, decreases sharply and flattens out in the frequency band of 250-1000 MHz. The permeability plots reveal the non-magnetic behavior of the concrete material; the real part of μ_r is close to the free space value ($\mu_r=1$) while the imaginary part is seen to be close to zero value. The slight variations in the curves may be attributed to the finite accuracy of the calibration and measurement process.

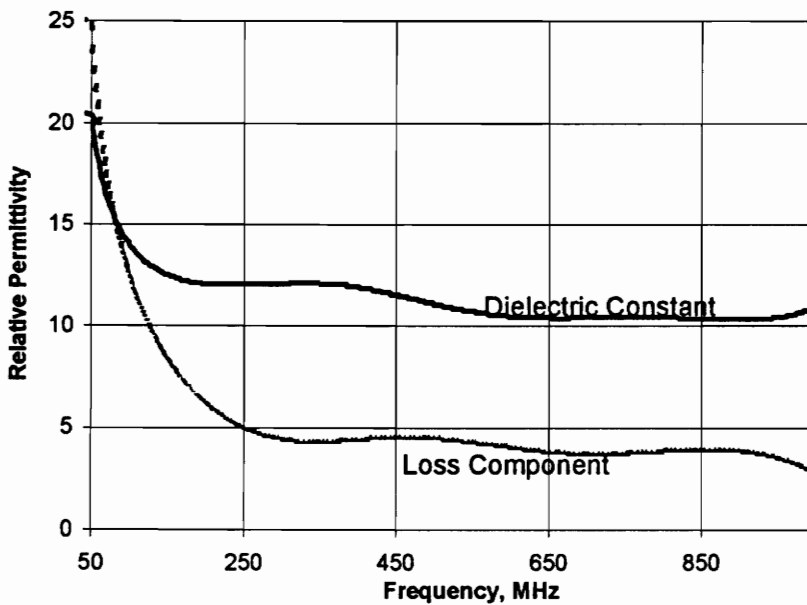


Figure 3.8 Relative permittivity plots of a PCC specimen.

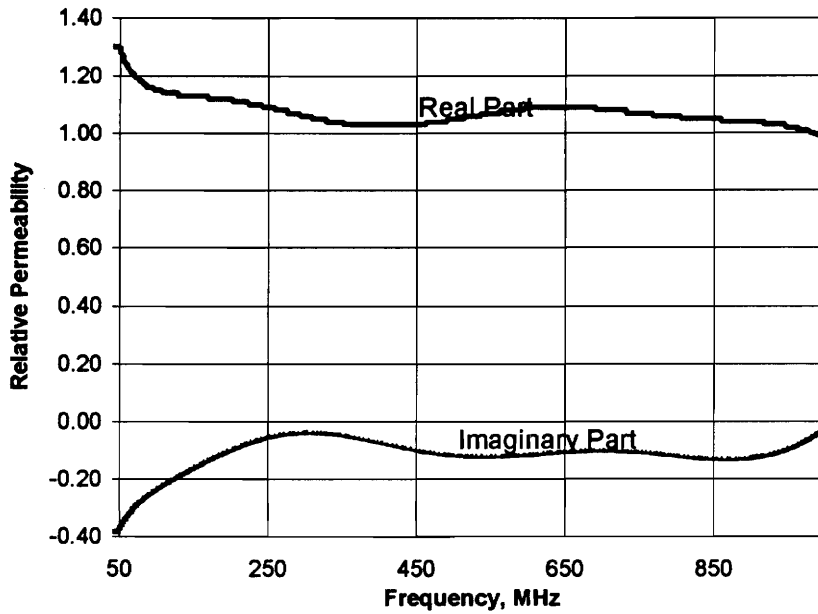


Figure 3.9 Relative permeability plots of a PCC specimen.

Another concrete specimen, about three months old, was characterized to see the changes in material properties due to aging. Figures 3.10 and 3.11 show the ϵ_r and μ_r curves for a specimen which is about three months old and has been kept in a dry condition. By comparison with figure 3.8, a drop in both the real and imaginary parts of ϵ_r is noticeable, the change being more significant in the imaginary part. The imaginary component represents loss in the specimen and the main source of this loss is water in concrete. For a concrete specimen which is kept in a dry condition, the water content will reduce with time and thus the loss will also reduce. This behavior is reflected in the curves.

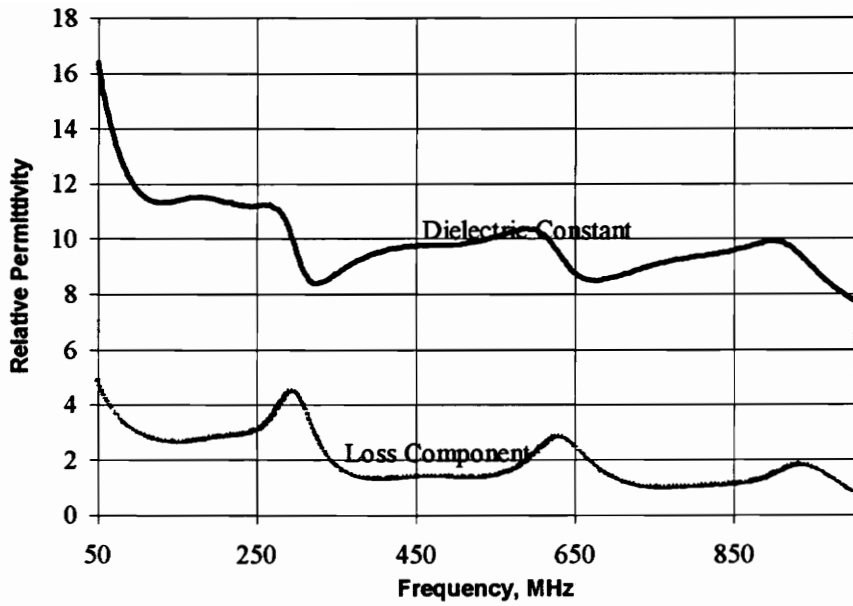


Figure 3.10 Relative permittivity plots of an old PCC specimen.

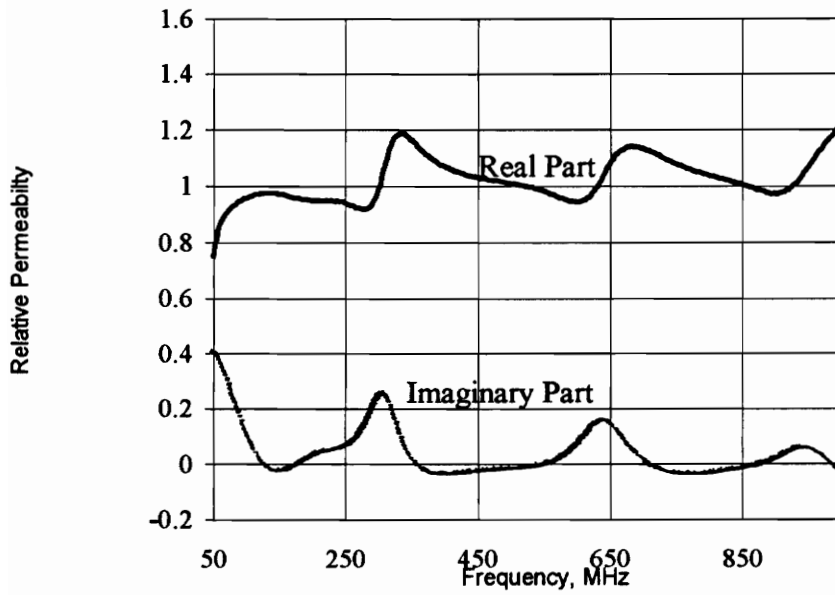


Figure 3.11 Relative permeability plots of an old PCC specimen.

CHAPTER 4

TIME DOMAIN DIELECTRIC

CHARACTERIZATION

4.0 INTRODUCTION

In this chapter, material characterization in time domain by the designed coaxial fixture is discussed. The concept of time domain measurement is introduced and different underlying principles involved in such measurements are discussed. Material characterization, an application in the field of time domain measurements is reviewed next. Then follows the presentation of the measurement technique used in the current research along with the experimental set up. The chapter concludes with the experimentally obtained results and discussions.

4.1 TIME DOMAIN MEASUREMENT: AN OVERVIEW

Time domain (TD) measurement is an attractive technique in terms of reduced complexity over frequency domain (FD) measurement and offers the observer to study the temporal behavior of a system. A physically realizable signal has valid representations in both time domain and frequency domain and characteristic features of a system in either domain can be exploited to serve specific purposes. In the context of measurement system, FD techniques imply CW operation with high degree of precision in measurement and calibration, involving great amount of time. TD techniques, on the other hand, can be simple, fast and also accurate at the same time. With the advent of present-day pulse generators and sampling oscilloscopes incorporating state-of-the-art digital technology, TD techniques offer an attractive and accurate measurement option. The wide field of TD measurements involve material characterization, remote sensing, broadband measurement

of electrical parameters of electrical equipment and pulse measurements for computer applications.

The fundamental elements in TD measurement setup are pulse generators and different classes of oscilloscopes. [32], [33] provide a rich discussion on these equipments. They are discussed only briefly in the following section:

•*Pulse Generator:*

A pulse generator provides a source of excitation to the measurement system. A pulse generator can be classified by the waveforms it generates and the transition duration characteristics of the waveshapes. The usual classes of waveshapes include step, truncated ramp, impulse and RF pulse. The spectral characteristics of these pulses are different from each other and frequency band of interest in a measurement setup dictates the choice of a particular waveshape. Different solid state devices incorporated in the electronic circuitry in the pulse generators can include step recovery diode (SRD), tunnel diode, microwave FET or bipolar transistors, Impatt diodes and superconducting Josephson junction switches.

•*Oscilloscopes:*

Oscilloscopes provide a means to display and/or record waveforms in a signal measurement environment. Two broad categories of this equipment are real time oscilloscopes and equivalent time oscilloscopes. For measurements at microwave frequencies, equivalent time sampling oscilloscopes are used. Such oscilloscopes include a feed through sampling head which can be remotely placed or mounted in the same unit.

The performance characteristic of a complete TD instrumentation setup is determined by its impulse response function $h(t)$. For a LTI system, $h(t)$ determines the output from the system to any input by the convolution operation. The system's response $h(t)$ is a composite of the responses from the following subsystems:

- *Transmission system:*

Connectors, cables connecting the signal source to the measurement plane.

- *Detector:*

Amplifiers in real time scopes or sampler in equivalent time scopes.

- *Display/Digitizer.*

The frequency response of $h(t)$ is an important element in that it can alter the temporal characteristics of the measured signal. Deconvolution techniques can be applied to extract the actual signal from the recorded output [34], [35].

The accuracy of a TD measurement setup is limited by two classes of errors, systematic and random errors. Reference [32] describes such errors associated with a TD measurement system. In the category of systematic errors are impedance mismatch, oscilloscope calibration nonlinearities and quantization errors involved in A/D conversion process. *S*-parameter measurement in TD involves establishment of reference impedance level and the quality of connecting cables and connectors play an important role in this case. The time base and the vertical scale calibration of the oscilloscope should be free from errors to ensure high accuracy of the system. Random errors include noise level, time base jitter and long term drifts.

4.2 TIME DOMAIN MEASUREMENT: CONCEPTS

Characteristics of wave propagation in a medium depends upon the electromagnetic (EM) properties of that medium. Wave propagation is supported by transmission lines, waveguide structures and free space radiation. To sustain wave propagation in the principal or transverse electromagnetic (TEM) mode, the electric and the magnetic field are oriented in the transverse plane in such a way that the Poynting vector points to the direction of propagation. When the propagating EM wave confronts a discontinuity (an interface between two adjacent medium), the orientation of the component fields change. This results in a redistribution of energy in the wave and some of the energy is contained in the reflected waveform and the rest is transmitted through the discontinuity. The electromagnetic properties like permittivity and permeability, of the two medium determine the amount of reflection and transmission at the interface. The component waves, reflected and transmitted waves contain information about the nature of the medium providing the discontinuity. Thus, if the transmitted and reflected signals along with the incident signal are recorded and analyzed, the EM properties of the medium can be evaluated. This is the fundamental principle of measurement in TD. The principle involves two basic concepts:

- Time Domain Reflectometry (TDR)
- Time Domain Transmission (TDT)

4.2.1 *Time Domain Reflectometry*

The discipline of TDR measurement is useful in characterizing materials enclosed in a an acknowledged electromagnetic configuration. TDR measurement consists of two distinct categories:

- TD Reflectometer
- TD Spectroscopy

TD Reflectometer:

It is basically a qualitative analysis system where the reflected waveforms are observed with regards to their shapes and delays. These observed characteristics are then related to spatial variations along the path of signal propagation. To an experienced observer, the time signatures or reflected waveforms reveal the nature of discontinuities and their locations. This information is valuable when a visual inspection/investigation is required. An example of this case is the use of a ground penetrating radar to investigate ground layers beneath the surface.

TD Spectroscopy:

When quantitative analysis regarding material properties is called for, TD spectroscopy can be employed. Here the observed waveforms are recorded/stored by a dedicated computer used in the measurement system. The waveforms are then processed according to an established mathematical model to yield the material properties. A variety of digital signal processing techniques, like sampling of waveforms, digital transformation methods, is an inherent part of the processing of the waveforms.

Principle:

The objective of material characterization is to investigate the frequency dependent behavior of a specific set of parameters of the material under test. This implies observing the response of the material under sinusoidal excitation of different frequencies. But in TD measurement, the scope of such a frequency sweep does not exist and the Fourier Transform is used to bridge the different realms of time domain and frequency domain behavior. The concept of time causality is employed here since the observation of the waveform before a certain time epoch, say $t=0$, is not important. The principle of TD measurement can be elucidated with reference to figure 4.1.

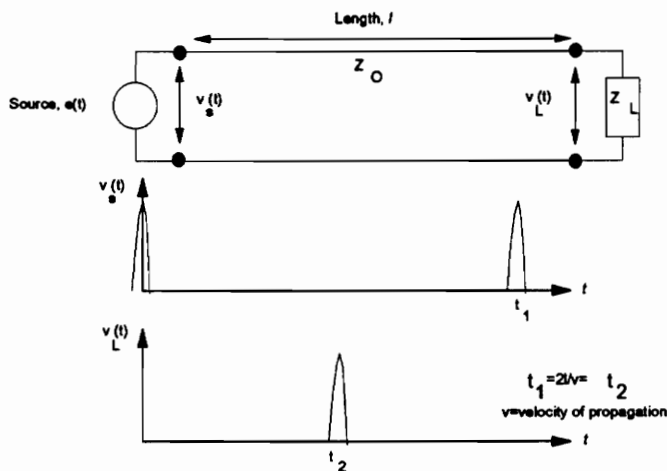


Figure 4.1 Concept of time delay for reflected waveforms.

In figure 4.1, a transmission line of length l and characteristic impedance Z_0 connects a load of impedance Z_L to a source of excitation $e(t)$. The source generates an impulse which travels down the transmission line to the load end. Depending upon the

mismatch between the Z_L and Z_0 , there will be some reflection and an impulse will reappear at the source end. The time delays t_1 and t_2 , as shown in that figure, will depend upon the length l and propagation characteristic of the transmission line. The lossy nature of the line will impose a bandlimited operation and will manifest itself in pulse broadening. The nature of the load termination can be obtained from the reflected waveform. Figure 4.2 shows a similar set up as in figure 4.1, but with a constant excitation source and different load terminations, open and short. The observed reflected waveforms at the source side are shown in the same figure.

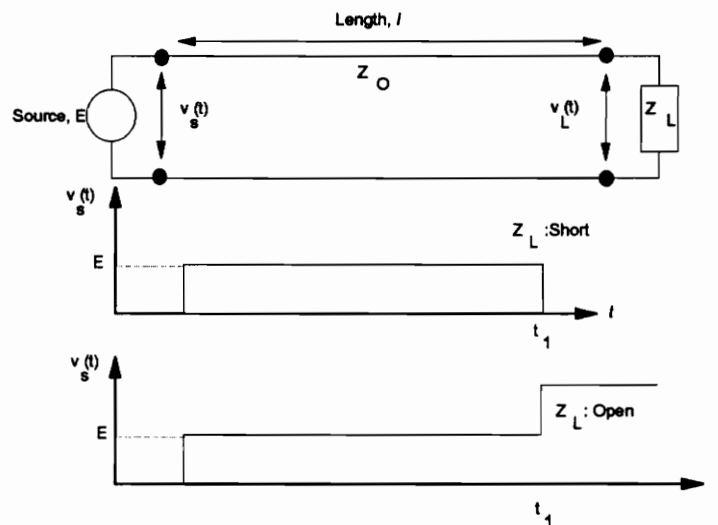


Figure 4.2 Voltage waveforms on a line for different load terminations.

For a short circuit termination, the incident signal experiences a reflection coefficient of (-1) , whereas for open circuit case, it experiences a unity $(+1)$ reflection

coefficient. The steady state voltage level at any point in the line is the superposition of the incident and reflected waveforms.

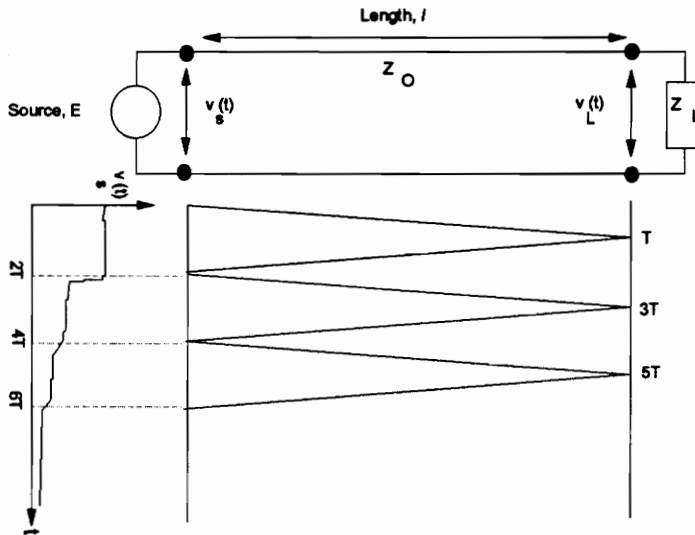


Figure 4.3 Use of RT diagrams in TDR.

RT diagram or commonly known as bounce diagram, is an important tool in analyzing multiple reflections in a transmission line. Figure 4.3 shows a modification of the set up in figure 4.1. The excitation source has impedance Z_s and $Z_s \neq Z_0$. The mismatch between Z_s and Z_0 will cause an initial reflection at the source side and the excitation seen by the line is $E(Z_0/(Z_0+Z_s))$. Reflections from the load end will arrive at the source end after a certain time delay and the voltage at the sending end, $v_s(t)$ will change in accordance with the superposition of reflected waveforms with the incident waveform. Multiple reflections will be present as seen from the same figure and they will arrive at the source side after an integral multiple of the first time delay. The subsequent

reflections will decay in amplitude and the signal $v_s(t)$ will settle down to some final value. The load end will experience transmitted waveforms to the load and also the reflections from the source at some later time. A discretely loaded transmission line can be analyzed by the RT diagram. In such a case, the analysis will be tedious as there will be multiple reflections from the different discontinuities along the length of the line. The type of load termination will determine the waveforms at different positions along the line. Thus the RT diagram can provide one with some initial analysis and about the expected waveforms in a TDR set up.

TDR Set up:

The principle of basic TDR set up is the same for both TD reflectometer and TD spectroscopy. A basic TDR system consists of the following:

- Pulse generator
- Sampling oscilloscope
- Reference Transmission line

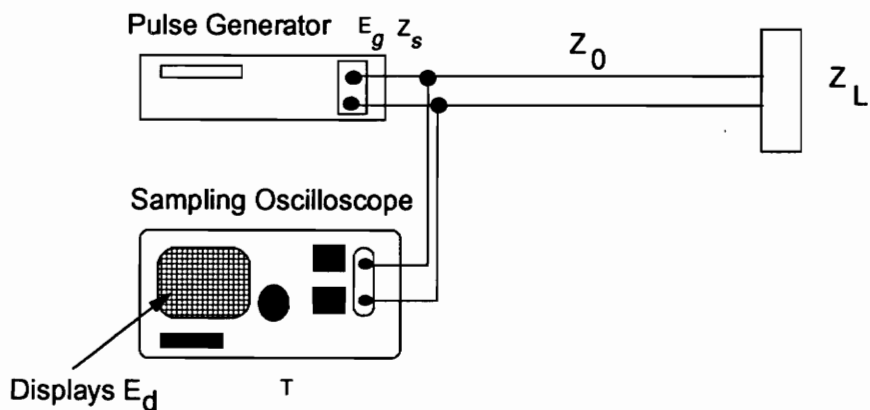


Figure 4.4 Basic TDR set-up.

Figure 4.4 shows the schematic representation of a basic TDR set up. In some cases, the pulse generator and the sampling oscilloscope can be merged into one single unit. The reference line should provide enough time delay to avoid overlapping of multiple reflections. The focus here is to obtain the reflection coefficient of the unknown load termination. This can be done by taking the following steps:

1. Short circuit termination by a highly reflective known standard termination. The TDR waveform is acquired by the sampling scope.
2. Matched load termination by a standard load of $Z_0(s)$. The acquired waveform gives the response of the load when it is matched to the reference line.
3. Load termination by an unknown load from the material under test.

These three waveforms are sufficient [39] to determine the $\rho_L(s)$ of the load and in addition, if $Z_0(s)$ is known, $Z_L(s)$ can be obtained from the knowledge of $\rho_L(s)$ and $Z_0(s)$ according to the equation

$$\rho_L(s) = \frac{Z_L(s) - Z_0(s)}{Z_0(s) + Z_L(s)} \quad (4.1)$$

A simple method can be adopted to calculate the S -parameter from the reflection measurement [32]. A suitable time window can be chosen which will include the transition in the incident waveform at the air-dielectric discontinuity excluding any subsequent reflection. With this choice of time window, the expression for the TDR waveform can be written in the s domain as

$$E_d(s) = E_g \frac{Z_0}{Z_0 + Z_s(s)} [e^{-\gamma l} \rho_r(s) e^{-\gamma l} (1 + \rho_s(s))] T(s) \quad (4.2)$$

where,

$E_d(s) = \mathcal{L}[e_d(t)]$, \mathcal{L} denoting Laplace Transformation,

$Z_s(s)$ = source impedance,

$\rho_r(s)$ = reflection coefficient at load end,

$\rho_s(s)$ = reflection coefficient at source end,

γ = propagation constant, and

$T(s)$ = transfer function of the oscilloscope.

If the coaxial line is terminated with a known reflection standard, preferably short circuit, $\rho_r(s)$ becomes (-1) and

$$E_{d,short}(s) = -E_g \frac{Z_0}{Z_L + Z_0} [e^{-2\gamma l} (1 + \rho_s(s))] T(s) \quad (4.3)$$

If the dielectric is inserted in the line, then the acquired TDR waveform is

$$E_{d,load} = E_g \frac{Z_0}{Z_0 + Z_s(s)} [e^{-\gamma l} S_{11} e^{-\gamma l} (1 + \rho_s(s))] T_s(s) \quad (4.4)$$

These two waveforms can be related to the S_{11} parameter

$$S_{11}(s) = -\frac{E_{d,load}(s)}{E_{d,short}(s)} \quad (4.5)$$

The set up and method of analysis assumes the presence of principal or fundamental mode. The reference line is designed so that it operates well below the cut-off point of higher order modes that might be present in other parts of the network.

4.2.2 Time Domain Transmission

Time domain transmission deals with transmitted waveforms rather than reflected waveforms. Transmitted waveforms carry the information about the type of discontinuity in their time signatures. This serves as a useful tool in material characterization. The

concept of TDT is based on the assumption of the representative network model for the discontinuity. One such model is based on the incorporation of scattering of electromagnetic waves and incorporates scattering or S -parameters. The discontinuity can be modeled as a two port network where the S -parameters determine the amount of reflection and transmission at the two ports.

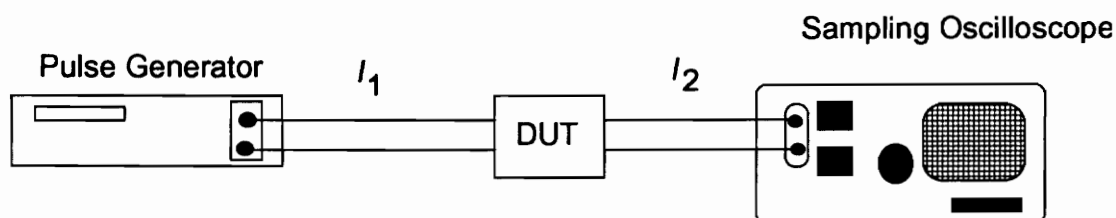


Figure 4.5 Basic TDT set-up.

The basic TDT system is shown in figure 4.5. Reference lines l_1 and l_2 are connected to one end, to the pulse generator and sampling oscilloscope, respectively. A device under test is inserted between two reference planes formed at the other ends of the reference lines. The pulse generator provides excitation signal to the DUT through reference line l_1 . The oscilloscope records the transmitted waveform through the DUT with appropriate time delay. The waveforms can provide one with a first hand knowledge about the transmission behavior of the inserted network. For complete characterization, one needs to determine all the S -parameters of the network model of the DUT. This

requires TD insertion measurement technique involving acquisition of the following waveforms:

1. TDR waveforms when the reference transmission lines are terminated in short standards. This yields the reflection standard.
2. TDT waveforms when the transmission lines are directly coupled together. This set up realizes the Thru standard.
3. Both TDT and TDR waveforms when the DUT is inserted between the reference planes. Often the DUT is enclosed in a standard transmission line configuration, so often an additional waveform is acquired with the empty enclosing section inserted between the reference planes. This realizes the Line standard.

With all these acquired waveforms, the S -parameters of the inserted network can be derived and the electromagnetic properties of the material under test can be evaluated.

For a TDT set up, a simple procedure similar to the one described in TDR section can be undertaken to evaluate S_{21} of a material [32]. Again a proper time window needs to be chosen to exclude the secondary reflections. Two waveforms need to be acquired in such a setup. The first one, the incident waveform, $v_{di}(t)$, is obtained by connecting the two reference lines together. Then the material under test is inserted between the lines and a transmitted waveform, $v_{dt}(t)$, is acquired. The ratio of these two waveforms in s domain yields the S_{21} of the material,

$$S_{21}(s) = \frac{V_{dt}(s)}{V_{di}(s)} \quad (4.6)$$

where,

$$V_{dt}(s) = \mathcal{L}[v_{dt}(t)],$$

$$V_{di}(s) = \mathcal{L}[v_{di}(t)].$$

Andrews [32] points out to the features of simple duration limited TD measurement of S -parameters. The attractive feature is that the frequency response parameters cancel out in the final expression for S_{11}/S_{21} . The pulse generator should provide a signal spectrum that is well above the system noise level. This simple technique is limited in the low frequency range, the lower end of the frequency response gets altered when the secondary reflections are neglected.

4.3 MATERIAL CHARACTERIZATION IN TIME DOMAIN

Feldegg [4-6] reported measurement of dielectric relaxation time for Debye dielectrics, permittivity and conductivity of materials in a TD measurement environment. The measurement set up is that of TDR, the material under test being inserted in a coaxial transmission line. The properties are evaluated in the range of 30 ps to 200 ns. Cole [7] reported measurement of complex permittivity from the analysis of reflected waveforms from a sample placed in a coaxial line. Nicolson and Ross [3] presented TDR setup to measure the S -parameters of the test specimen and relating them to the intrinsic properties of the material. Stuchly and Matuszewski [37] provides a mathematical treatment whereby the dielectric properties can be related to the S -parameters of a specimen. The

measurement technique is a combined reflection-transmission method and can be implemented in TD by broadband network analyzers.

There is a number of ways to implement TD measurement of dielectric material. One of them involves the common microwave insertion technique where the material under test contained in a transmission line, is inserted between two reference lines. Or one can resort to one port measurement techniques based on TDR setup. Based on the set up, either TDR or TDT or a combination of both suffices to provide the required information. For one port measurement involving precision line, there are several possible options for TDR set up [2]:

- Test specimen placed in a reference line of impedance Z_0 and is terminated by another line of impedance of Z_0 .
- Test specimen placed in a reference line of impedance Z_0 and is terminated by a short circuit.
- Test specimen placed in a reference line of impedance Z_0 and is backed by another dielectric material of known ϵ_r .

In all cases, the TDR signature is acquired in a time window long enough to accommodate all possible multiple reflections. Mathematical analysis is different in three cases. All the above mentioned methods are based on the assumption of unity relative permeability for the test material, because a knowledge of the reflected waveform is not enough to determine two unknowns, ϵ_r and μ_r . The accuracy of a particular method depends upon the sample thickness and the value of the dielectric constant of the sample.

Simulation results show that [2] the first method is suitable for low dielectric constant while the second method, for high dielectric constant. The dielectric constant is represented in a series expansion in the methods above and truncation is required to limit the number of terms and get an approximate result. A thin material suffers from high noise level but the truncation errors are negligible upto some high frequencies. A thick material is associated with low noise level but suffers from truncation errors at low frequencies.

When a material needs to be characterized from both permeability and permittivity point of view, a simultaneous acquisition of reflected and transmitted waveforms is required. Reference [3] describes a set up for such purpose. A sample holder accommodates the sample and is backed by a reference line terminated in a short circuit. Though the basic set up is that of TDR, the short circuit provides a doubly transmitted signal through the sample. The time signatures acquired in different time windows provide a knowledge of the S -parameters as a function of frequency. The assumption here is that the material is reciprocal.

There is a one port measurement technique possible for dielectric characterization, which assume an infinitely long specimen. If a specimen is infinitely long in the direction of signal propagation, there will be no secondary reflection from the specimen except for the first reflection from the air-dielectric interface. For such a case, the specimen can be modeled by a one port network containing only S_{11} parameter and the reflection coefficient ρ is equivalent to S_{11} [25]. The assumption of infinitely long specimen can be

realized in practice by time domain gating techniques. The TDR waveforms are gated (equivalently windowed by a rectangular window) so that the tails settle to some value and then acquired. Figure 4.6 shows the schematic representation of this gating technique.

The expression for S_{11} is then

$$S_{11}(j\omega) = \rho(j\omega) = \mathcal{F}[v_r(t)]/\mathcal{F}[v_i(t)] \quad (4.7)$$

where \mathcal{F} denotes Fourier Transform operation.

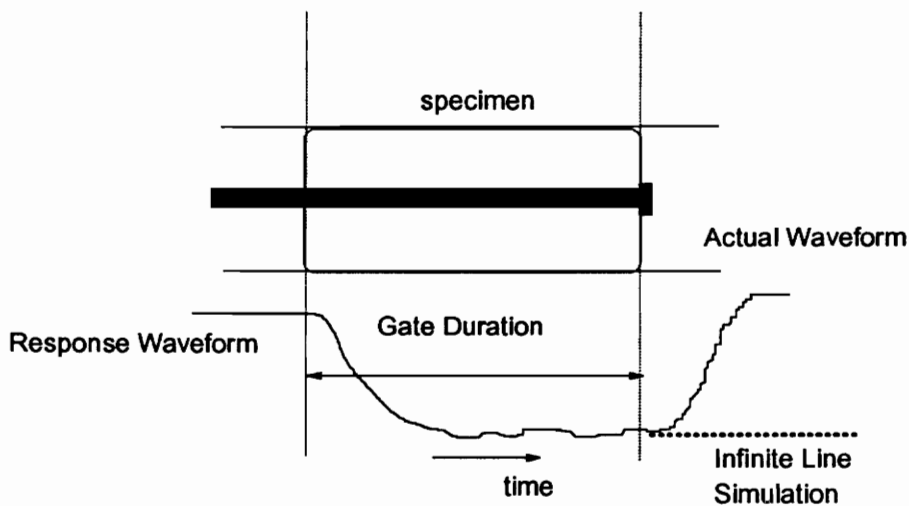


Figure 4.6 Gating technique.

In terms of impedance, $\rho(j\omega)$ can be expressed as shown in equation 4.1. If a coaxial air transmission line of impedance Z_0 is filled with a material of permittivity ϵ_r and permeability μ_r , Z_0 gets modified in the following way

$$Z_0' = \frac{Z_0}{\sqrt{\frac{\mu_r}{\epsilon_r}}} \quad (4.8)$$

If the section of the transmission line filled with test specimen, acts as a termination, then Z_0' presents itself as the load impedance. The expression for ρ , equation 4.1 can be rearranged to yield the following expression

$$\rho = \frac{1/\sqrt{\frac{\mu_r}{\epsilon_r}} - 1}{1/\sqrt{\frac{\mu_r}{\epsilon_r}} + 1} = \frac{\sqrt{\epsilon_r} - \sqrt{\mu_r}}{\sqrt{\epsilon_r} + \sqrt{\mu_r}} \quad (4.9)$$

From equation 4.7 we can write,

$$S_{11} = \frac{\sqrt{\epsilon_r} - \sqrt{\mu_r}}{\sqrt{\epsilon_r} + \sqrt{\mu_r}} \quad (4.10)$$

If the μ_r of the specimen is assumed to be unity,

$$S_{11} = \frac{\sqrt{\epsilon_r} - 1}{\sqrt{\epsilon_r} + 1} \quad (4.11)$$

From which we can write,

$$\epsilon_r = \left(\frac{1 - S_{11}}{1 + S_{11}} \right)^2 \quad (4.12)$$

where,

$$S_{11} = \mathcal{F}[v_r(t)/v_i(t)].$$

4.4 FOURIER TRANSFORM

As mentioned earlier, the classical Fourier Transform bridges the time domain and the frequency domain representation of any physical signal. In a TD measurement set up, waveforms are acquired and stored and subsequently analyzed by a computer. This requires a discrete time representation of the waveforms. An analog signal $v(t)$ is sampled with equal intervals and the sampling rate has to be above the Nyquist rate to preserve the

spectral contents of the original signal. The Fourier transform is approximated by the discrete Fourier Transform (DFT) as given below

$$v(nT) = \frac{1}{N} \sum_{k=0}^{N-1} V(k\Omega) e^{jkn\Omega T} \quad (4.13a)$$

$$V(k\Omega) = \sum_{n=0}^{N-1} v(nT) e^{-jkn\Omega T} \quad (4.13b)$$

where,

Ω is the fundamental discrete frequency

T is the sampling interval

N is the number of discrete data points.

The computation of DFT yields frequency components which are approximate representations of the continuous time Fourier Transform. Certain restrictions need to be fulfilled to maintain high accuracy in the computation of frequency components by DFT. The computation of DFT is based on the assumption that the sampled waveform is periodic with a period of T_w , the acquisition window size. But in TD measurement involving step waveforms, this condition is hardly satisfied. The initial and final values are not same and the DFT produces truncation errors. There are several ways to circumvent this difficulty. One simple way is to take the average of the initial and final values and replace the final value by this average. One can also take the derivative of the step waveform to produce a duration limited periodic waveform. But the problem with this method is that it gives rise to high noise level. Another possibility is to subtract a linear ramp from the step waveform so that the initial and the final values are the same. The dc component computed this way is not accurate. One way to introduce periodicity in a step

waveform is to flip the signal in a manner described in [38]. The even frequency components are zero calculated this way and [36] provides a mean to obtain a complete and accurate frequency domain representation by combining the ramp and Gans method.

Fast Fourier Transform (FFT) is used here to compute the DFT components of a signal.

4.5 DIELECTRIC SPECTROSCOPY OF CONCRETE WITH THE FIXTURE

4.5.1 Principle:

A research has been undertaken to study the behavior of concrete during its curing period and also under different external conditions. To study the material properties of concrete under different treatments, more than one specimen was cast for each treatment, for example, different types of aggregates, different water to cement ratio, freeze-thaw, alkali-silica reaction etc. to reduce variability among the specimens. This resulted in a large number of test specimens and an efficient, accurate and time-wise economical measurement was sought for to characterize all the specimens. After investigating several possible techniques, one-port TD measurement was used. One-port measurement technique offers a simplified measurement configuration where insertion and removal of test specimens and recordings of relevant waveforms can be done in a short period of time. This is important when a batch process with a large number of specimens is involved in measurements. The accuracy is also satisfactory with such measurements.

The principle used in this set up is that of 1 port measurement technique involving gating of waveforms. This technique has been chosen on the assumption of free-space permeability ($\mu_r=1$) for the test specimen. This assumption of unity permeability can be justified from the permeability plots in figures 3.9 and 3.11. Thus the number of unknowns (material properties) reduce to one (ϵ_r only) and a reflected waveform (from the specimen) along with the incident waveform is sufficient to yield ϵ_r . This principle has been described in the previous section and equation 4.12 shows the final expression of ϵ_r in terms of the acquired waveforms.

4.5.2 Measurement Set up:

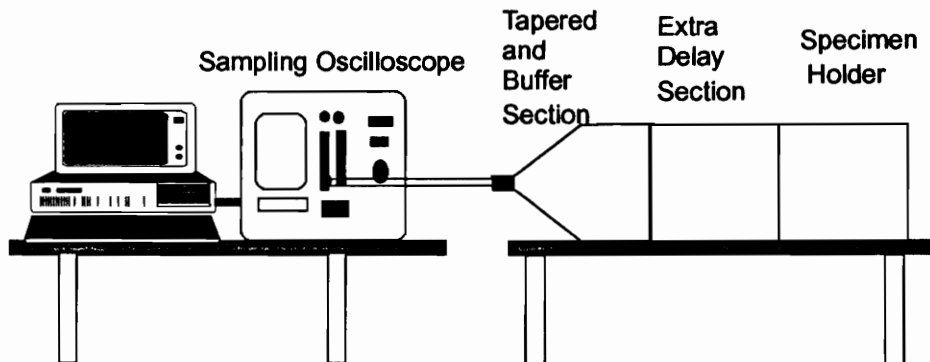


Figure 4.7 Experimental set-up.

The TD one port measurement set up is shown in figure 4.7. The set up comprises of the following apparatuses:

- Digital Sampling Oscilloscope

- Coaxial Fixture
- Computer Interface

Digital Sampling Oscilloscope:

The sampling oscilloscope used in this measurement set up is Tektronix 11801. This instrument includes the feature of feed thru sampling heads and a pulse generator. A step pulse is used for the source excitation with rise time 15.2 ps. The scope provides as many as 8 channels and several numerical processing functions such as differentiation, averaging etc.

Coaxial Fixture:

The designed coaxial fixture is used in a modified form in this measurement set up. The modified fixture consists of one tapered section, and a buffer section, followed by an extra delay line and finally the specimen holder. The extra delay line is included to obtain sufficient time delay between successive multiple reflections from the specimen under test. The specimen is terminated in open circuit (air). A short circuit termination would have been a better option considering the frequency dependent capacitance associated in open circuit termination [21], but due to the mechanical difficulties in aligning the metal plate and achieving a good contact, this could not be applied.

Computer:

An IBM pc was interfaced with the sampling oscilloscope to download the digitized data. A complete program written in BASIC language was used to store the displayed waveforms from different channels. The data was saved in an ASCII format.

4.5.3 Procedure:

The measurement procedure consisted of acquiring a reference or incident waveform and a response waveform from the test specimen. The time window was chosen such that the waveform containing the transition due to the first reflection only from the front face was included. The end of the extra delay line formed the reference plane for measurement. The incident waveform on this plane was acquired by placing the circular brass plate at the end of the extra delay line. The response waveform is acquired by connecting the specimen holder and placing the specimen in it. These two waveforms can be processed to yield the frequency dependent complex permittivity of the test specimen.

4.5.4 Results:

Dielectric characterization in time domain with the designed coaxial fixture was done on a number of concrete specimens. Teflon was used as a test material to validate the measurement technique in terms of accurate results. The reference and response waveforms were acquired within a 2 ns time window. This window size was adequate to exclude the secondary reflections. Figure 4.8 shows the frequency dependent behavior of relative permittivity of Teflon for a frequency range of (100 MHz- 1 GHz). The real part or the dielectric constant is close to 2.0 for the frequency range of interest and shows a little peak at around frequency 500 MHz. This may be attributed to the non-gradual change in the inner geometry of the tapered section, deviations from cylindrical shape of

the specimen holder and the buffer section due to machining, mechanical misalignment associated with the insertion and removal of the test specimens. The dielectric constant of Teflon is reported as 2.0 [40] so that the deviation over the bandwidth is 2% while the maximum deviation is about 10% and occurs around 500 MHz. The loss component or imaginary part is seen to hug the frequency axis or zero value closely, which is a true indication of negligible dielectric losses present in Teflon.

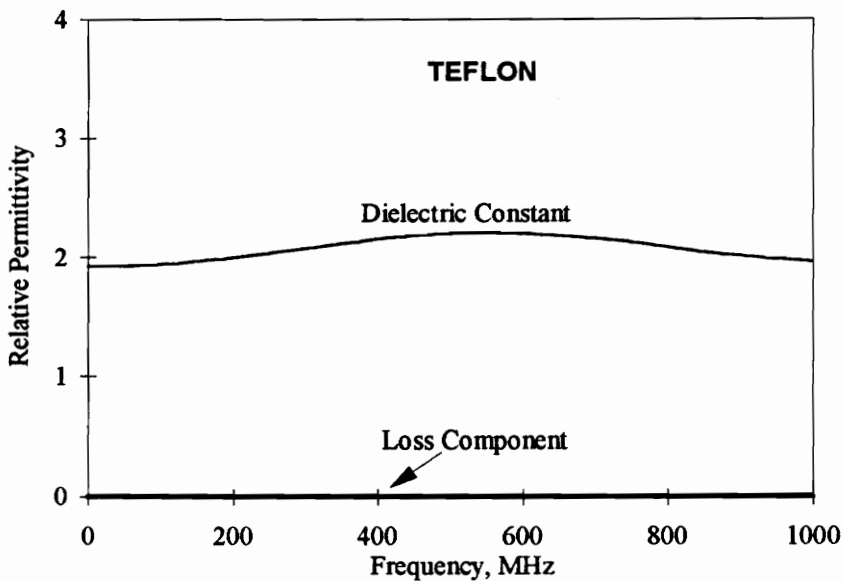


Figure 4.8 Relative permittivity plots for Teflon.

Concrete specimens of different mixes and at different times during its curing period were tested for dielectric spectroscopy using the coaxial fixture. A time window of 3 ns was chosen in this case. Because concrete has higher dielectric constant than Teflon,

therefore the velocity of signal propagation is slower and thus a longer time delay for the secondary reflections. A plot of the acquired reference and response waveforms for a typical concrete specimen is shown in figure 4.9. The evaluated relative permittivity from processing these waveforms are shown in figure 4.10. The dielectric constant has a drooping characteristic in the earlier portion of the frequency range and settles down to some final value for the remaining portion. The loss component of relative permittivity exhibits a rising characteristic in the low frequency range and then rolling off to some minimum value in the high frequency range. The anomalous behavior in the low frequency range is due to the truncation of the waveforms such that the low frequency behavior is altered. If all the multiple reflections have been included in the acquired waveforms, the low frequency behavior would have been correctly represented.

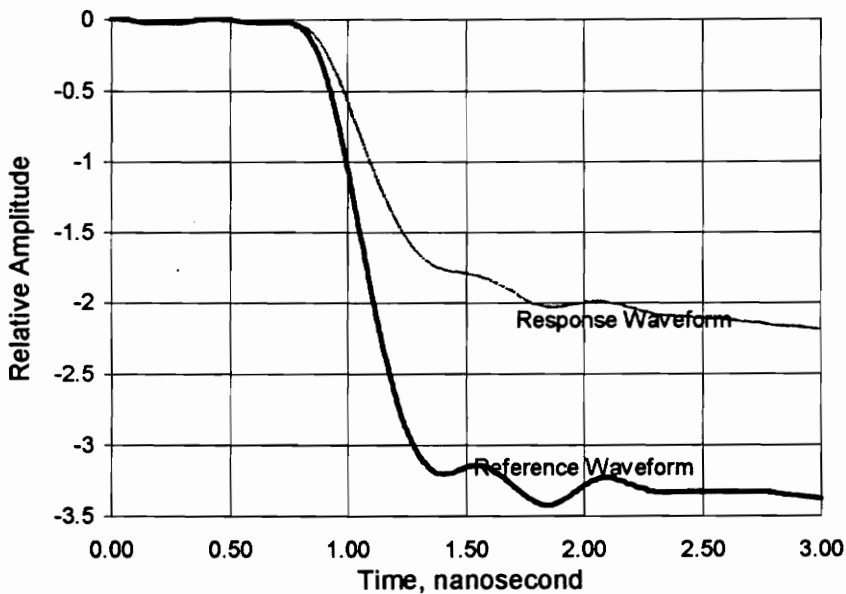


Figure 4.9 Time waveforms for simplified one-port measurement.

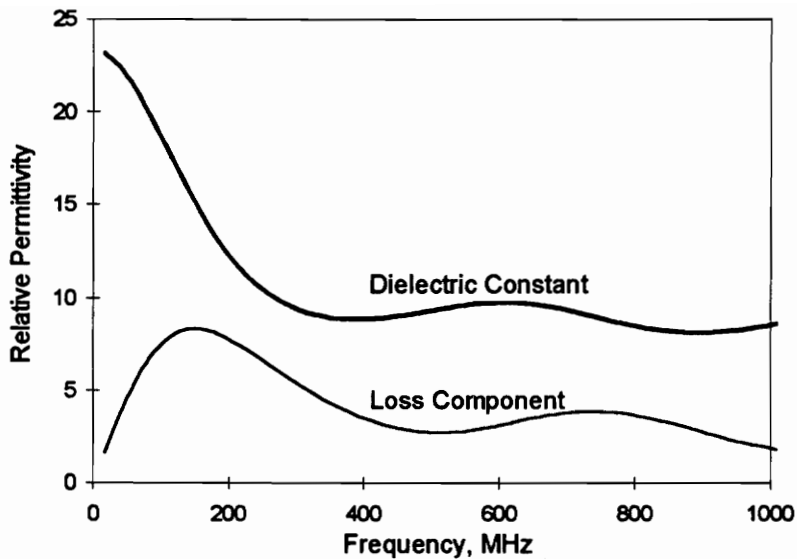


Figure 4.10 Relative permittivity plots for a concrete specimen.

A study was done on the designed coaxial fixture to examine the variability of the simplified one-port measurement process. A particular concrete specimen, which was kept in dry condition for a long period of time, was chosen as the reference specimen. Because of the condition of the specimen, it could be safely assumed that there would be no variations of ϵ_r with time. At different days, the specimen was characterized for ϵ_r . Based on the average and the variance of the measurements, a 95% confidence interval bound was calculated for both the dielectric constant and the loss component. Figure 4.11 shows the average values and the confidence interval bound for both components of ϵ_r as a function of frequency. The loss component being very small for a dry specimen is seen to vary within small limits around the zero value. The bounds show that the measurements

are repeatable within a small interval. Thus the statistical behavior of the measurement process reveals its repeatability nature.

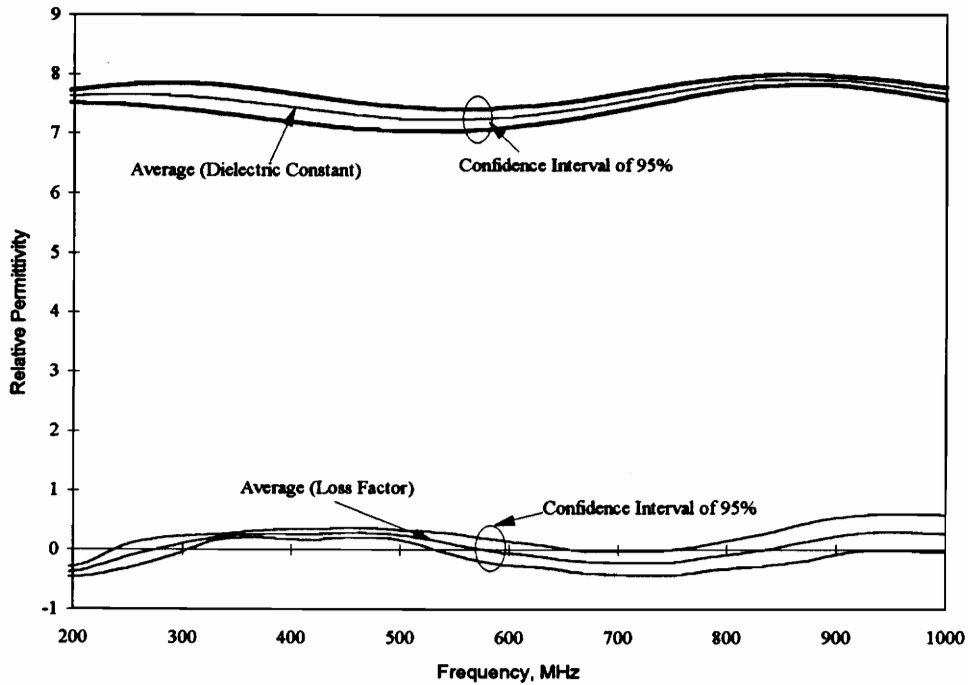


Figure 4.11 Variability study on the simplified one-port measurement process.

It might be of interest to study the change of ϵ_r of concrete material with curing time as obtained by the measurement process. A concrete specimen after being cast, is put into curing room for moisture curing. The specimen is tested for ϵ_r at some particular interval of days. Figure 4.12 shows the variation in dielectric constant and figure 4.13 shows the variation of loss component with time at some specific frequencies. It is more informative to study the relative changes at specific frequencies rather than over the whole spectrum. The loss component is seen to be more sensitive to curing time than the

dielectric constant and the changes are noticeable at early stages of the curing period and at lower frequencies. As concrete matures after being cast, water content gets reduced by internal mechanism. Water is the main contributor to the loss component ϵ_r'' of concrete and its reduction with time is reflected in the plots in figure 4.13. The main components of the concrete being stable in composition do not undergo noticeable change. This behavior is shown in the relatively stable plots of ϵ_r' in figure 4.12.

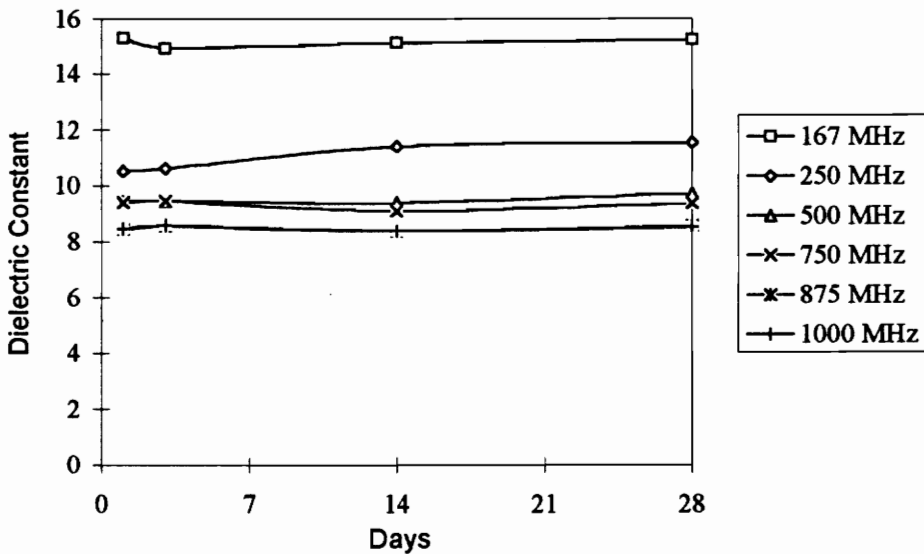


Figure 4.12 Variation of dielectric constant of concrete with curing time.

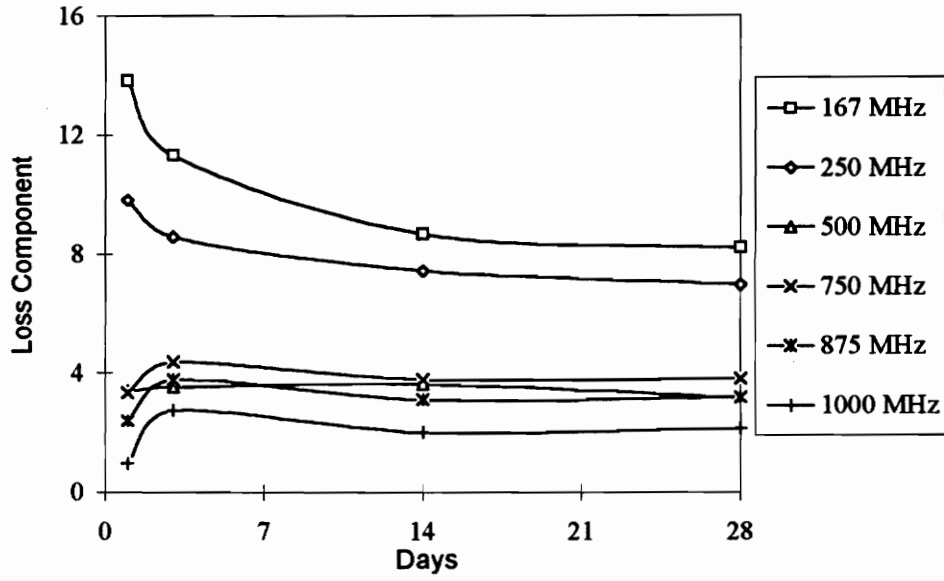


Figure 4.13 Variation of loss component of concrete with curing time.

CHAPTER 5

TIME DOMAIN CALIBRATION AND

DE-EMBEDDING

5.0 INTRODUCTION

In the previous chapter, simplified one port measurement was discussed and the permittivity plots obtained by this method exhibited inaccuracy in the low frequency region. To circumvent that problem, a TDR measurement method which includes calibration and de-embedding, is discussed. The chapter starts with evaluation of S -parameter of the fixture and determination of ϵ_r of the test specimen by taking into consideration of these parameters. This is basically the process of calibration and de-embedding and this has been done in time domain environment. A method, based on the extension of the de-embedding process, is proposed to correct the permittivity plots obtained from the simplified one port measurement.

In a microwave measurement set up, the device under test (DUT) is connected to the measuring instruments through embedding network. The embedding network may include connecting cables, fixtures and RF probes. The actual scattering parameters of the DUT get modified by the scattering parameters of the embedding network. De-embedding is the inverse of this modification or transformation process, which is intended to yield the actual S -parameter of the DUT from a knowledge of S -parameter of the embedding network. Calibration is the process whereby the S -parameter of the embedding network are evaluated as a function of frequency. Wideband de-embedding process in frequency domain with standard terminations has been reported by Vaitkus [26]. Bauer [27] discusses de-embedding in terms of Z -parameters for a single port device. Lane provides a variety of de-embedding techniques to evaluate device

S-parameters [28]. A generalized method for de-embedding of multi-port networks is formalized by Sharma [29]. Lance discusses an error analysis for de-embedding process at microwave frequencies [41]. Steinhelfer [30] discusses de-embedding in time domain by employing gating techniques to separate multiple reflections. Su [31] presents a complete calibration process for both TDR and TDT applications. The same author discusses de-embedding process in time domain for different load terminations [21].

5.1 TD CALIBRATION FOR MODELING THE FIXTURE

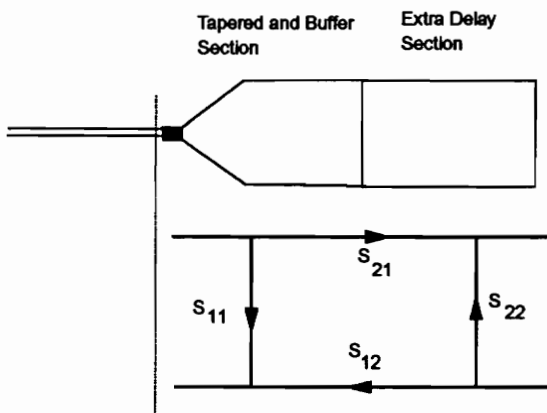


Figure 5.1 *S*-parameter model for the fixture.

Figure 5.1 shows the coaxial fixture without the specimen holder, along with its representative *S*-parameter model. The front end of the tapered section forms the measurement plane. The free end of the extra delay line forms the load plane where different loads of known reflection coefficient are connected. We need three different load terminations to derive the *S*-parameters, namely:

- Short circuit termination.
- Open circuit termination.
- Matched load termination.

The reflected waveforms acquired under the above load terminations along with the incident waveform are sufficient to yield S_{11} , S_{22} and S_{12} . S_{21} as a function of frequency. The necessary mathematical background is presented below:

Short termination:

In this case, $\Gamma = -1$. We can write

$$\begin{aligned} V_{sh} &= V_{in} \left[S_{11} + \frac{S_{12} \cdot S_{21} \cdot \Gamma}{1 - S_{22} \Gamma} \right] \\ &= V_{in} \left[S_{11} - \frac{S_{12} \cdot S_{21}}{1 + S_{22}} \right] \\ \frac{V_{sh}}{V_{in}} &= S_{11} - \frac{S_{21} \cdot S_{12}}{1 + S_{22}} \end{aligned} \quad (5.1)$$

Open circuit termination:

In this case, $\Gamma = 1$. We can write,

$$\frac{V_{op}}{V_{in}} = S_{11} + \frac{S_{21} \cdot S_{12}}{1 - S_{22}} \quad (5.2)$$

Matched load termination:

With the fixture terminated in its characteristic impedance, we have $\Gamma = 0$. Thus

$$\frac{V_m}{V_{in}} = S_{11} \quad (5.3)$$

If V_{in} , V_{sh} , V_{op} and V_m are known, the above equations can be solved for S_{11} , S_{22}

and S_{12} . S_{21} in terms of the TDR waveforms as follow

$$S_{11} = \frac{V_m}{V_{in}} \quad (5.4)$$

$$S_{22} = \frac{V_{sh} + V_{op} - 2V_m}{V_{op} - V_{sh}} \quad (5.5)$$

$$S_{21}.S_{12} = \frac{V_{op} - V_m}{V_{in}}(1 - S_{22}) \quad (5.6)$$

Thus to evaluate the frequency dependent S -parameters, one needs to evaluate the different waveforms in frequency domain. Figure 5.2 shows the schematic arrangement for obtaining the required waveforms. The process of acquiring the required waveforms is presented next.

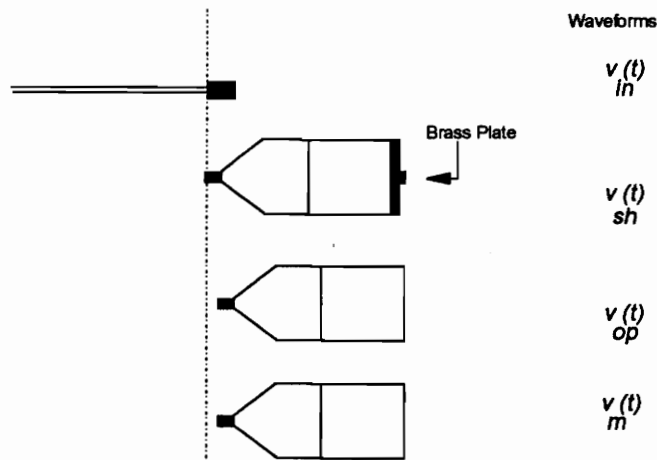


Figure 5.2 Time domain calibration standards.

Incident waveform, V_{in} :

This waveform is acquired by connecting a standard short termination at the end of the connecting cable. The acquired waveform in this case is $-v_{in}(t)$ because of the short termination. Then

$$V_{in} = \mathcal{F}[v_{in}(t)] \quad (5.7)$$

where \mathcal{F} denotes Fourier transform.

Reflected Waveform (Short Termination), V_{sh} :

This waveform is acquired by connecting the circular brass plate at the end of the fixture. As before, this is assumed as a highly reflected load and the acquired waveform is $v_{sh}(t)$. Then

$$V_{sh} = \mathcal{F}[v_{sh}(t)] \quad (5.8)$$

Reflected Waveform (open termination), V_{op} :

This waveform is acquired by keeping the free end of the fixture open. The load seen by the fixture is open space (air) and the Γ can be assumed to be unity. The waveform acquired is $v_{op}(t)$ and

$$V_{op} = \mathcal{F}[v_{op}(t)] \quad (5.9)$$

Reflected Waveform (matched termination), V_m :

To realize a matching standard, we resort to gating technique. The process does not involve any physical load termination and is based on simulation of a waveform resulting from a matched termination. This is done by tailoring either $v_{sh}(t)$ or $v_{op}(t)$ waveform. In this research, $v_{sh}(t)$ is truncated just before the falling edge from the first reflection and the waveform is made flat for the rest of the duration. This simulated waveform, $v_m(t)$, is to be expected to result from a matched termination and

$$V_m = \mathcal{F}[v_m(t)] \quad (5.10)$$

In the measurement, a time window of 80 ns was chosen to include all the possible multiple reflections and for the waveform to settle to some constant value after all the reflections die out. Fourier transform of these step waveforms are carried out as explained

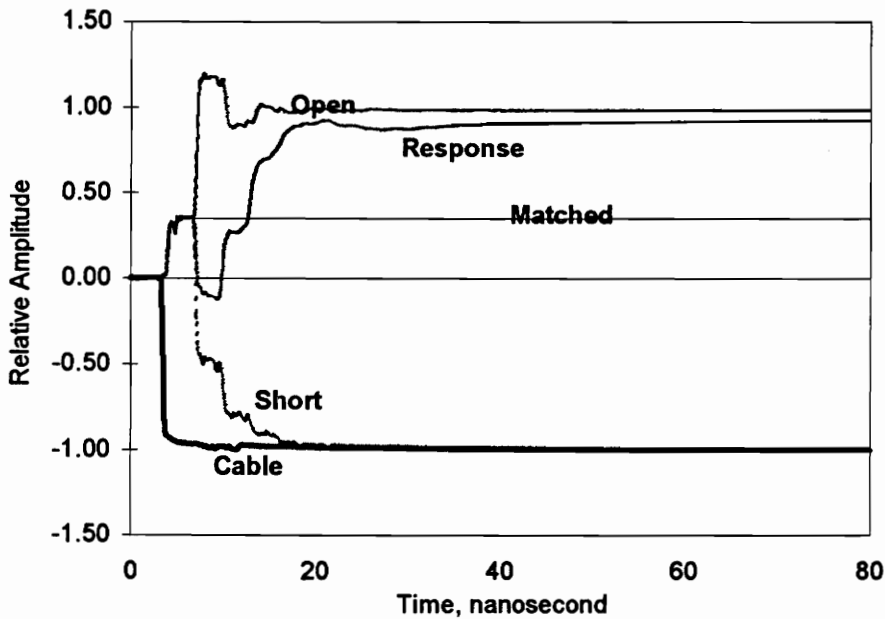


Figure 5.3 Different waveforms associated with TD calibration.

in the previous chapter. Figure 5.3 shows the different TDR waveforms acquired for calibration. Figure 5.4 shows the magnitude response of the S -parameters while figure 5.5 shows the phase response.

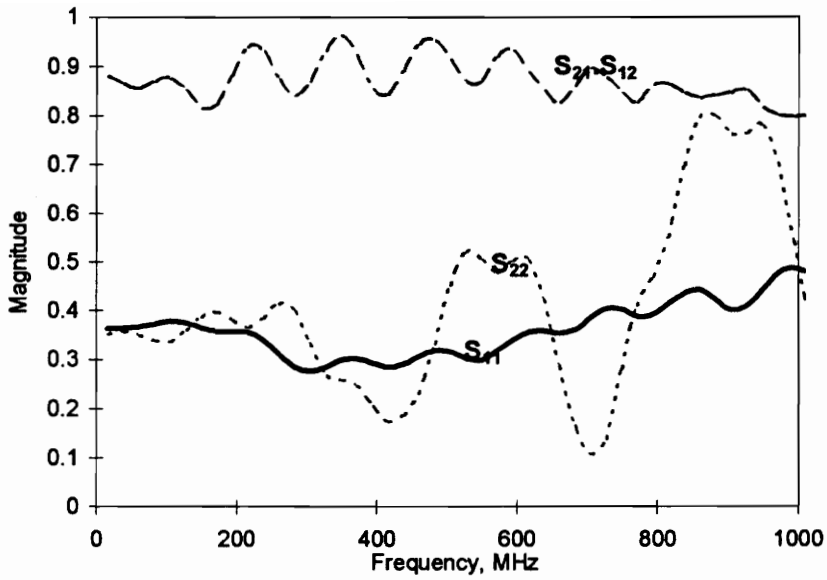


Figure 5.4 Magnitude plots of S -parameters of the fixture.

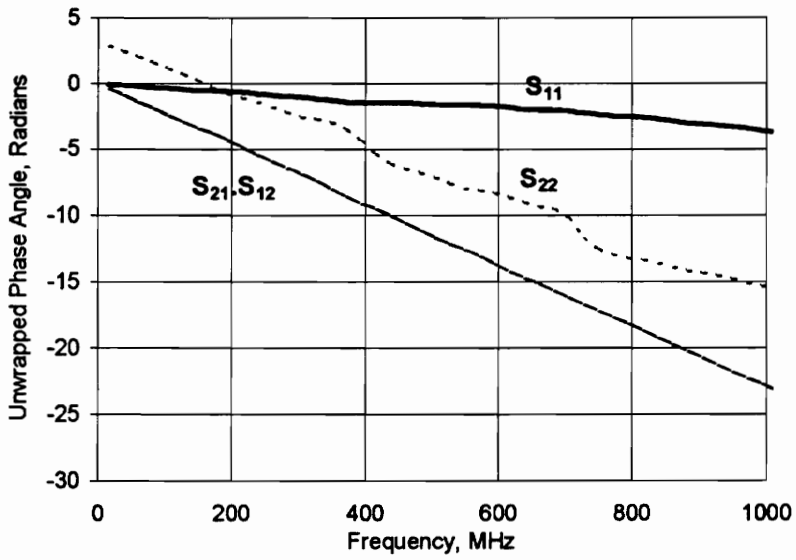


Figure 5.5 Phase angle plots of S -parameters of the fixture.

5.2 DE-EMBEDDING PROCESS

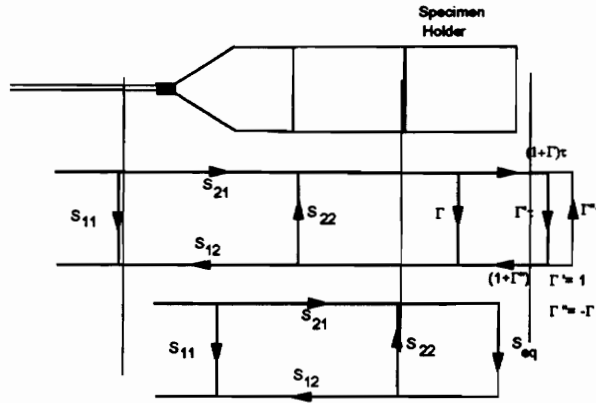


Figure 5.6 S-parameter model of the fixture with the specimen.

Figure 5.6 shows the specimen holder containing a test specimen, connected to the fixture. The S -parameter model is also represented along side the fixture. The specimen holder is represented by the signal flow graph and is in cascade with the network model of the fixture. The free end of the specimen holder is assumed to have open (air) termination. To write an expression for V_{res} in terms of V_{in} and the S -parameters, we need to simplify the network model. The signal flow graph can be reduced as shown in figure

5.6. S_{eq} can be expressed as

$$S_{eq} = \frac{x - x.e^{2\alpha x} - e^{2\alpha x} - 1}{-1 - x - e^{2\alpha x} + x.e^{2\alpha x}} \quad (5.11)$$

where $x = \sqrt{\epsilon_r}$,
 $\alpha = -j\frac{\omega}{c}d$

The details of the derivation is given in the appendix. The specimen is assumed to have $\mu_r \cong 1$.

V_{res} can be related to V_{in} through the network parameters as follows,

$$\frac{V_{res}}{V_{in}} = S_{11} + \frac{S_{21}.S_{12}.S_{eq}}{1 - S_{eq}.S_{22}} \quad (5.12)$$

The expression can be rearranged to form the following transcendental equation in x ,

$$S_{21}.S_{12} \left[\frac{S_{eq}}{1 - S_{22}.S_{eq}} \right] - \left[\frac{V_{res}}{V_{in}} - S_{11} \right] = 0 \quad (5.13)$$

where S_{eq} is given in equation 5.11.

With a knowledge of the S -parameters of the fixture, the incident waveform $v_{in}(t)$ and the response waveform $v_{res}(t)$ from the specimen, the transcendental equation can be solved for x and thus for ϵ_r .

5.3 VERIFICATION:

The de-embedding process developed above can be verified in terms of V_{res} from the known values of V_{in} , ϵ_r and the S -parameters of the fixture. This verification process is done in frequency domain. The expression for V_{res} can be written as (equation 5.12)

$$V_{res} = V_{in} \left[S_{11} + \frac{S_{21}.S_{12}.S_{eq}}{1 - S_{22}.S_{eq}} \right] \quad (5.14)$$

Let the response waveform be $V_{res,sim}$ when all the variables in the right hand side of equation 5.14 are plugged in for their values. Let the measured response waveform be $V_{res,meas}$. Thus to validate the de-embedding process, we need

$$V_{res,sim} = V_{res,meas} \quad (5.15)$$

A TDR waveform $v_{res}(t)$ from a test specimen was acquired for the de-embedding process. S -parameters of the fixture were derived as discussed in the previous section. Equation 5.13 was solved for ϵ_r of the specimen and the results are shown in figure 5.7.

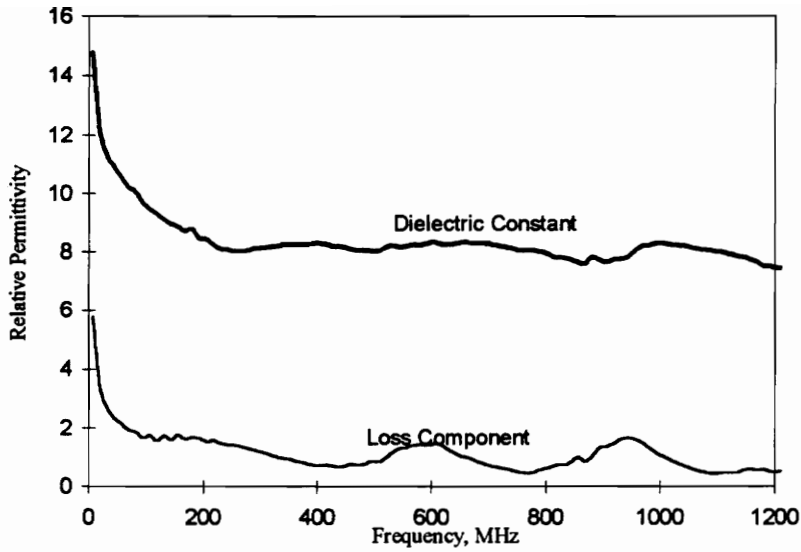


Figure 5.7 Relative permittivity plots from de-embedding process.

The non-smoothness of the plots for ϵ_r' and ϵ_r'' are due to the numerical solutions of the equation 5.13. The loss component is seen now to exhibit a decrease in the low frequency range and gradual settling down in the remaining frequency band. This is to be expected for the loss component of relative permittivity of a material like concrete. Figures 5.8 and 5.9 show the magnitude and phase comparison plots of $V_{res,sim}$ and $V_{res,meas}$. The closeness of the plots validate the de-embedding process.

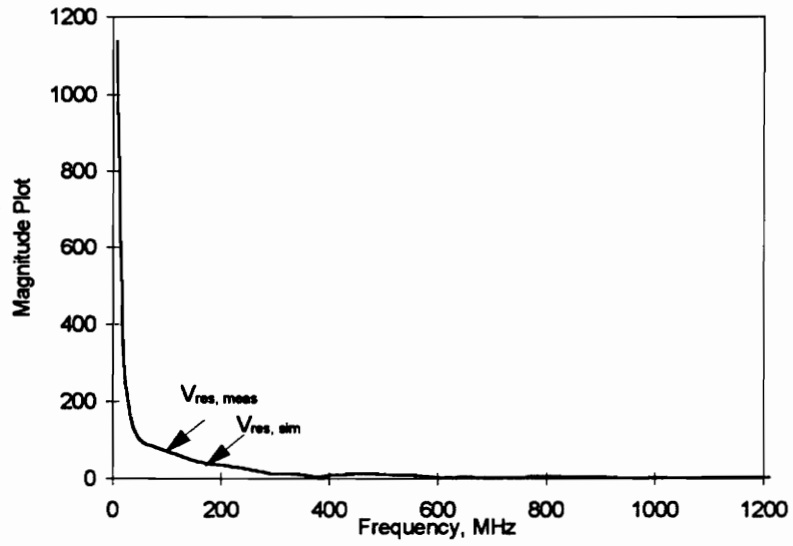


Figure 5.8 Magnitude plots for simulated and response waveforms.

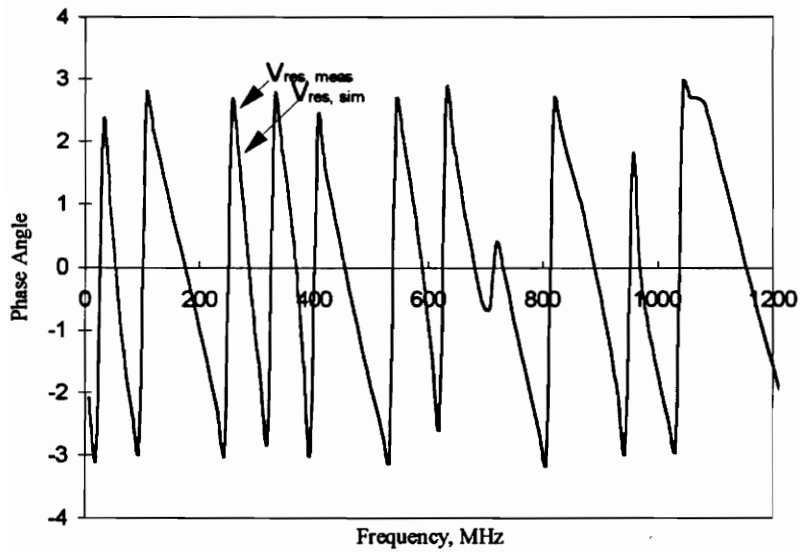


Figure 5.9 Phase angle plots for simulated and measured waveforms.

5.4 SENSITIVITY ANALYSIS

A sensitivity analysis was done on the measurement technique based on de-embedding procedure. The analysis is based on generating frequency domain simulated response for deviations from actual values of ϵ_r and comparing these responses with the measured one to see the effects of these deviations in ϵ_r . This analysis focuses on the sensitivity or resolution capability of the measurement technique. The analysis starts with the numerical solution of equation 5.13 in terms of ϵ_r . Then ϵ_r is varied as $\epsilon_r' = \epsilon_r \pm \Delta\epsilon_r$, where, $\Delta\epsilon_r$ is some arbitrary deviation. In the analysis, $\Delta\epsilon_r$ is chosen as 10% and 30% of ϵ_r . The responses $V_{res, sim}$ are generated from these values of ϵ_r' through equation 5.14. Figure 5.10 shows the relative changes in magnitude of the simulated responses compared to the measured one while figure 5.11 shows the changes in phase angles. From the changes of the magnitude plots, it can be seen that changes are prominent in the high frequency region (>300 MHz). The phase is sensitive to change in ϵ_r at some particular frequencies. Thus, to notice a change in the response waveform due to a change in ϵ_r , one needs to concentrate on the spectral components in the high frequency end. Hence the sensitivity of using this scheme for evaluation of ϵ_r is not uniform over the frequency range of interest. It is clear that for most of the 300-900 MHz range, the sensitivity is fairly adequate to yield a good estimate for the PCC dielectric constant.

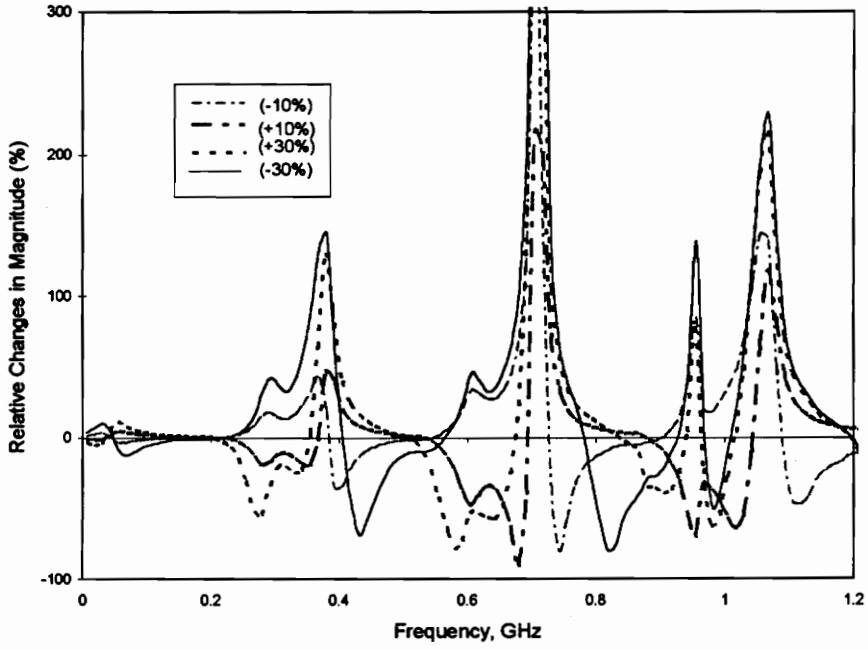


Figure 5.10 Relative changes in magnitude of simulated responses.

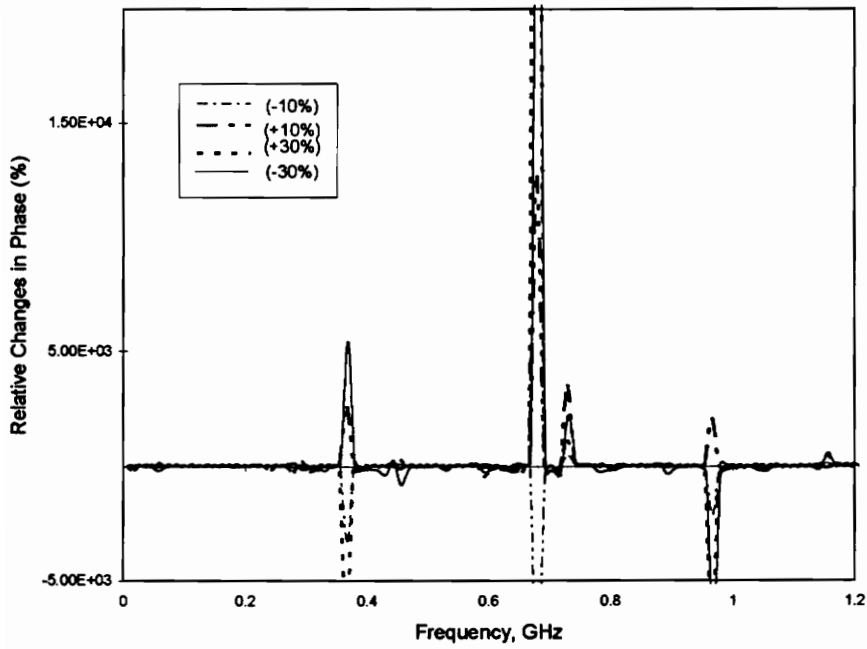


Figure 5.11 Relative changes in phase angle of simulated responses.

5.5 EXTENSION OF THE DE-EMBEDDING PROCESS

As has been shown in the previous chapter, the simplified one port measurement technique is based on the first reflection from the specimen and excludes subsequent multiple reflections. The exclusion of the secondary reflections result in an alteration of the low frequency behavior and the loss component particularly shows anomalous behavior by a rising curve in the low frequency range. In this section, a method is proposed to correct the relative permittivity plots obtained from the simplified one port measurement based on S_{11} only. This involves TD calibration and de-embedding process described in the previous section.

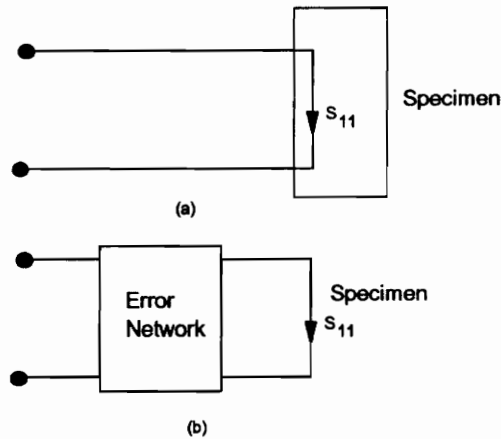


Figure 5.12 (a) S-parameter model for simplified one-port technique. (b) Actual model.

We begin by illustrating in figure 5.12 the network model under the simplified one port measurement and its actual representation. Figure 5.12 (a) shows that the effect of

the convolution of the fixture (multiplication in frequency domain) is neglected in evaluating S_{11} . But as shown in figure 5.12 (b) the actual S_{11a} gets modified by the intermediate network termed here as error network to yield S_{11e} . Thus the simplified one port technique measures S_{11e} , which is related to S_{11a} by

$$S_{11e} = S_{err} \cdot S_{11a} \quad (5.16)$$

where S_{err} is the transfer characteristics of the error network.

Now S_{11a} can be obtained by performing de-embedding operation with a test specimen. S_{11a} can be obtained from the calculated ϵ_r by the following expression

$$\epsilon_r = \left(\frac{1 - S_{11a}}{1 + S_{11a}} \right)^2,$$

hence, $S_{11a} = \frac{1 - \sqrt{\epsilon_r}}{1 + \sqrt{\epsilon_r}}$ (5.17)

where ϵ_r is obtained from the de-embedding process.

If the same specimen is measured by the simplified one port measurement technique, we obtain the S_{11e} . With S_{11e} and S_{11a} known, S_{err} can be determined from equation 5.16 as

$$S_{err} = \frac{S_{11e}}{S_{11a}} \quad (5.18)$$

To de-embed this S_{err} from the simplified one port measurement, let a specimen be evaluated for its S_{11} as S_{11}' . To obtain the actual parameter S_{11a}' , we need to resort to the equation 5.18

$$S_{11a}' = \frac{S_{11}'}{S_{err}} \quad (5.19)$$

With the correct value of S_{11}' , S_{11a}' evaluated, we can get the corrected ϵ_{ra}' as follows

$$\epsilon'_{ra} = \left(\frac{1 - S'_{11a}}{1 + S'_{11a}} \right)^2 \quad (5.20)$$

To apply the proposed correction process, a particular test specimen is characterized by both simplified and complete (de-embedding) one port measurement method. This yields S_{err} . Then any other specimen which has already been characterized by the simplified method, is corrected by applying S_{err} . The waveforms from the simplified measurement need to be extended to the proper length (time duration of the waveforms in the calibration and de-embedding process) so that the frequency points in S_{11}' and S_{err} (equation 5.19) match. This involves zero padding of the waveforms before performing the FFT. Figure 5.13 shows the relative permittivity plots with and without the correction process. The jittery behavior can be attributed to the accumulation of errors in the numerical solution of the transcendental equation, division in frequency domain. Other than a change in the magnitude, both the corrected real and imaginary components exhibit the general trend as the uncorrected components and the corrected loss component does not show the anomalous behavior in the low frequency any more.

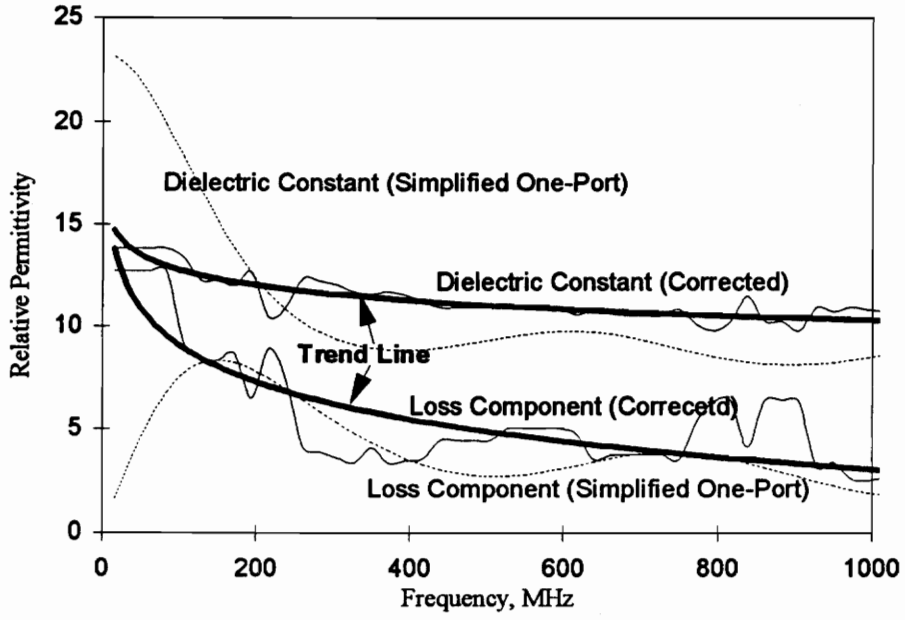


Figure 5.13 Relative permittivity plots from correction process.

CHAPTER 6
CONCLUSIONS

6.0 SUMMARY

A coaxial transmission line fixture has been designed to be used in a measurement set up for material characterization of concrete. Wideband microwave measurements in both frequency domain and time domain are used in this work. The measurement techniques have been investigated with emphasis on their use in impedance measurements. The research mainly focused on time domain measurements and calibration. De-embedding techniques in time domain have been studied. A correction process based on de-embedding process has been proposed to rectify the approximate time domain measurements.

A coaxial fixture was designed with an intent to study the material properties of concrete. To simulate the assessment of concrete in practical structures, test specimens were fabricated to accommodate aggregate sizes of the order of one (1) inch. This resulted in the design of a coaxial fixture of large dimensions and of characteristic impedance of 100Ω . Adapter sections in the form of conical coaxial transmission line were designed to connect the fixture to the 50Ω connecting cables and instruments. Frequency domain measurements employed two port insertion measurement. A vector network analyzer (HP 8510 B) was used as the measuring instrument and the calibration scheme was based on TRL (Thru, Reflection, Line) principle. The expressions used for ϵ_r and μ_r in terms of the reflection coefficient and the transmission coefficient are derived in chapter three.

Time domain measurement was based on one-port measurement or S_{11} measurement. Dielectric spectroscopy was investigated using the first reflection technique based on gating the reflection from only the front face of the specimen. Test specimen of reference material such as Teflon, was characterized by this technique to check the accuracy. This simplified technique provided an analytical expression for ϵ_r in terms of the measured waveforms. More elaborate model for the fixture and the specimen was investigated using the concept of time domain calibration and de-embedding process. This resulted in evaluation of the S -parameters of the fixture. The calibration process yielded S_{11} , S_{22} and S_{21} . S_{12} from three measurements with known load terminations. The ϵ_r of the test material was de-embedded from these S -parameters by iterative solution of a transcendental equation.

6.1 RESULTS AND CONCLUSIONS

Frequency domain measurement results were obtained after calibration and material properties were obtained as a function of frequency. The results indicated the change of material properties of concrete during different stages of its life period. The results also revealed that the concrete can be assumed to have free space permeability ($\mu_r \cong 1 - j0$). Based on this finding, a one-port measurement technique in time domain was adopted for dielectric characterization of concrete. Teflon was tested by this technique to examine the accuracy of the measurement process. Concrete specimen was tested to study the variability of the measurement process and the statistical analysis demonstrated

good repeatability. The effect of curing period on concrete was investigated and the effect was found to be more pronounced in the loss component ϵ_r'' than in the dielectric constant. An elaborate time domain calibration and de-embedding process was proposed to circumvent the loss of accuracy in low frequency range of the measurement bandwidth. The proposed model was validated by comparing the measured and the simulated response waveforms. A sensitivity analysis was done to study the changes in response waveforms for changes in ϵ_r . From the study of magnitude and phase angle plots in this analysis, it was seen that the effect of change of ϵ_r on the waveforms are prominent in the high frequency range. The de-embedding process was extended to come up with a correction process to correct for the low frequency errors from simplified one port measurement. Results show agreement between the general trend of the ϵ_r plots before and after correction, over the whole bandwidth.

APPENDIX

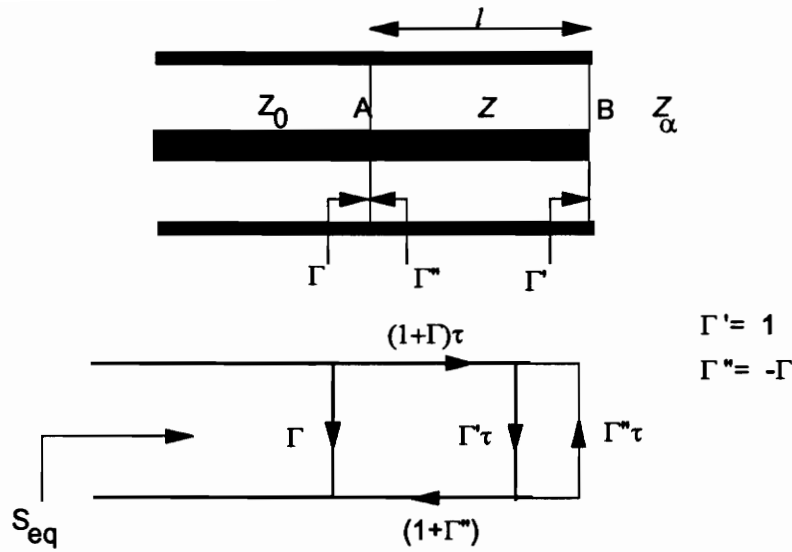


Figure A.1 Signal flow graph for the specimen.

In this section, the expression for S_{eq} (equation 5.11) will be derived. Figure A.1 shows the schematic of a coaxial line. The line contains a dielectric filling of permittivity ϵ_r for some length l . The line has air or open termination. The line is of impedance Z_0 and the section which contains the dielectric, the impedance is Z . The reflection coefficients at the different interfaces can be defined in terms of the relevant impedances as follows

$$\Gamma = \frac{Z - Z_0}{Z + Z_0} \quad (\text{A.1})$$

$$\Gamma'' = \frac{Z_0 - Z}{Z_0 + Z} = -\Gamma \quad (\text{A.2})$$

$$\Gamma' = \frac{Z_\infty - Z}{Z_\infty + Z} = 1 \quad (\text{A.3})$$

Let us define a term τ which takes into account the propagation in the material as

$$\tau = e^{-\frac{\omega}{c} \sqrt{\mu_r \epsilon_r} l} \quad (\text{A.4})$$

where ω is the radian frequency, c is the free-space speed of light, and μ_r and ϵ_r are the relative permeability and permittivity respectively. If the dielectric material is assumed to have $\mu_r=1$, then τ can be expressed as

$$\tau = e^{\alpha x} \quad (\text{A.5})$$

where $x = \sqrt{\epsilon_r} l$ and $\alpha = -j\frac{\omega}{c}l$.

Equation A.1 can be rearranged on terms of x as

$$\Gamma = \frac{1 - \sqrt{\epsilon_r}}{1 + \sqrt{\epsilon_r}} = \frac{1 - x}{1 + x} \quad (\text{A.6})$$

A signal flow graph representation of the coaxial line is also shown in figure A.1.

The equivalent S -parameter, S_{eq} , looking into face A, can be written as

$$S_{eq} = \Gamma + \frac{(1 + \Gamma)\tau(1 + \Gamma')\Gamma' \tau}{1 - (\Gamma' \tau)(\Gamma'' \tau)} \quad (\text{A.7})$$

After putting in the expressions for different Γ s, the expression above can be simplified as

$$S_{eq} = \frac{\Gamma + \tau^2}{1 + \Gamma\tau^2} \quad (\text{A.8})$$

The numerator and denominator of equation A.8 can be simplified as

$$\Gamma + \tau^2 = \frac{1 - x + e^{2\alpha x} + xe^{2\alpha x}}{1 + x} \quad (\text{A.9a})$$

$$1 + \Gamma\tau^2 = \frac{1 + x + e^{2\alpha x} - xe^{2\alpha x}}{1 + x} \quad (\text{A.9b})$$

Thus the final expression for S_{eq} is given as

$$S_{eq} = \frac{x - 1 - e^{2\alpha x} - xe^{2\alpha x}}{-1 - x - e^{2\alpha x} + xe^{2\alpha x}} \quad (\text{A.10})$$

REFERENCES

- [1]. Bussey, H. E., "Measurement of RF Properties of Materials, A Survey," Proceedings of the IEEE, pp. 1046-1053, June 1967.
- [2]. Shaarawi, A. M., "Dielectric Characterization using Time Domain Techniques," MS. Thesis, Department of Electrical Engineering, Virginia Polytechnic Institute and State University, June 1984.
- [3]. Nicolson, A. M. and Ross, G. F., "Measurement of Intrinsic Properties of Materials by Time Domain Techniques," IEEE Transactions on Instrumentation and Measurement, vol. IM-19, no. 4, pp. 377-382, November 1970.
- [4]. Fellner-Feldegg, H., "The Measurement of Dielectrics in Time Domain," Journal of Physical Chemistry, vol. 73, no. 3, pp. 616-623, March 1969.
- [5]. Fellner-Feldegg, H. and Barnett, E.F., "Reflection of a Voltage Step from a Section of a Transmission Line Filled with Polar Liquid," Journal of Physical Chemistry, vol. 74, no. 9, pp. 1962-1965, April 30, 1970.
- [6]. Fellner-Feldegg, H., "A Thin-sample Method for the Measurement of Permeability, Permittivity, and Conductivity in the Frequency and Time Domain," Journal of Physical Chemistry, vol. 76, no. 15, pp. 2116-2112, 1972.
- [7]. Cole, R.H., "Evaluation of Dielectric Behavior by Time Domain Spectroscopy. II. Complex Permittivity," Journal of Physical Chemistry, vol. 79, no. 14, pp. 1469-1474, 1975.
- [8]. Shaarawi, A. M., Riad, A. A., and Riad, S. M., "Time Domain Spectroscopy of Layered Dielectric Materials," CPEM 84 Digest, Deff, Holland, pp. 265-266, August 1984.
- [9]. Fidanboyly, K. M., Riad, S. M., and Riad, A. A., "An Enhanced Time-Domain Approach for Dielectric Characterization using Stripline Geometry," IEEE Transactions on Instrumentation and Measurement, vol. IM-41, no. 1, pp. 132-136, February 1992.
- [10]. Fidanboyly, K. M., Riad, S. M., and Riad, A. A., "A New Time-Domain Approach for Determining the Complex Permittivity using Stripline Geometry," IEEE Transactions on Instrumentation and Measurement, vol. IM-39, no. 6, pp. 940-944, December 1990.
- [11]. Al-Qadi, I. L., Riad, S. M., Mostafa, R. and Su, W., "Design and Evaluation of a Coaxial Transmission Line Fixture to Characterize Portland Cement Concrete," Proceeding of the 6th International Conference on Structural Faults and Repairs, UK, pp. 337-347, 1995.

- [12]. Mehta, P. K., *Concrete: Structure, Properties and Materials*, Englewood Cliffs, N.J., Prentice Hall, 1986.
- [13]. Whittington, H.W. and Wilson, J. G., "Low-frequency Electrical Characteristics of Fresh Concrete," IEE Proceedings, vol. 133, Part A, No. 5, pp. 265-271, July 1986.
- [14]. Al-Qadi, I. L., Hazim, O. A., Su W., Al-Akhras, N. and Riad, S. M., "Variation of Dielectric Properties of Portland Cement Concrete during Curing Time over Low RF Frequencies," Transportation Research Paper No. 940479, 73rd Annual Meeting, January 1994.
- [15]. Al-Qadi, I. L., Su, W., Riad, S. M., and Mostafa, R. and Hazim, O. A., "Coaxial Fixture Development to Characterize Portland Cement Concrete," Proceedings of the Symposium and Workshop on Time Domain Reflectometry in Environment, Infrastructure and Mining Applications, SP 19-94, Illinois, pp. 443-452, 1994.
- [16]. Wilson, J. G. and Whittington, H. W., "Variations in the Electrical Properties of Concrete with Change in Frequency," IEE Proceedings, vol. 137, Part A, no. 5, September 1990.
- [17]. Chew, W. C., Olp, K. J. and Otto, G. P., "Design and Calibration of a Large Broadband Dielectric Measurement Cell," IEEE Transactions on Geoscience and Remote Sensing, vol. 29, no. 1, pp. 42-47, January 1991.
- [18]. Nelson, R. E. and Coryell, M. R., "Electrical Parameters of Precision, Coaxial, Air-dielectric Transmission Lines," NBS Monograph 96, June 30, 1966.
- [19]. Chipman, R. A., *Theory and Problems of Transmission Lines*, Schaum's Outline Series, McGraw Hill Book Company, New York, NY, 1968.
- [20]. Ramo, S. and Whinnery, J. R., *Fields and Waves in Modern Radio*, John Wiley and Sons, Inc., New York, NY, 1944.
- [21]. Su, W., "Calibration of Time Domain Network Analyzers," Ph. D. Dissertation, Virginia Polytechnic Institution and State University, December 1992.
- [22]. Engen, G. F. and Hoer, C. A., "Thru-Reflection-Line: An Improved Technique for Calibrating the Dual Six-port Automatic Network Analyzer," IEEE Transaction on Microwave Theory and Techniques, vol. MTT-27, no. 12, pp. 987-993, December 1979.
- [23]. Hewlett-Packard, *HP 8510-B Network Analyzer Operating and Programming Manual*, Santa Rosa, California, 1988.

- [24]. Hewlett-Packard, *Customer Education: Basic Network Measurements Using the HP 8510-B Network Analyzer System*, Santa Rosa, California, 1988.
- [25]. Miller, E. K., *Time Domain Measurements in Electromagnetic*, Van Norstrand Reinhold Company, New York, NY, 1986.
- [26]. Vaitkus, R. L., "Wide-band De-embedding with a Short, an Open, and a Through Line," *Proceedings of the IEEE*, vol. 74, no. 1, pp. 71-74, January 1986.
- [27]. Bauer, R. F. and Penfield Jr., P., "De-embedding and Unterminating," *IEEE Transactions on Microwave Theory and Techniques*, vol. MTT-22, no. 3, pp. 282-288, March 1974.
- [28]. Lane, R., "De-embedding device Scattering Parameters," *Microwave Journal*, pp. 149-156, August 1984.
- [29]. Sharma, P. C. and Gupta, K. C., "A Generalized Method for De-embedding of Multiport Networks," *IEEE Transactions on Instrumentation and Measurement*, vol. IM-30, no. 4, pp. 305-307, December 1981.
- [30]. Steinhelfer Sr., H. E., "Discussion of De-embedding Techniques using Time Domain Analysis," *Proceedings of the IEEE*, vol. 74, no. 1, pp. 90-94, January 1986.
- [31]. Su, W. and Riad, S. M., "Calibration of Time Domain Network Analyzers," *IEEE Transactions on Instrumentation and Measurement*, vol. IM-42, no. 2, pp. 157-161, April 1993.
- [32]. Andrews, J. R., "Automatic Network Measurements in the Time Domain," *Proceedings of the IEEE*, vol. 66, no. 4, pp. 414-423, April 1978.
- [33]. Lawton, R. A., Riad, S. M. and Andrews, J. R., "Pulse and Time Domain Measurements," *Proceedings of the IEEE*, vol. 74, no. 1, pp. 77-81, January 1986.
- [34]. Parruck, B. and Riad, S. M., "An Optimization Criterion for Iterative Deconvolution," *IEEE Transactions on Instrumentation and Measurement*, vol. IM-32, no. 1, pp. 137-140, March 1983.
- [35]. Bennis, A. and Riad, S. M., "Filtering Capabilities and Convergence of the Van-Cittert Deconvolution Technique," *IEEE Transactions on Instrumentation and Measurement*, vol. 41, no. 2, pp. 246-250, April 1992.
- [36]. Shaarawi, A. M. and Riad, S. M., "Computing the Complete FFT of a Step-Like Waveform," *IEEE Transactions on Instrumentation and Measurement*, vol. IM-35, no. 1, pp. 91-92, March 1986.

- [37]. Stutchly, S. S. and Matuszweski, M., "A combined Total Reflection-Transmission Method in Application to Dielectric Spectroscopy," *IEEE Transactions on Instrumentation and Measurement*, vol. IM-27, no. 3, pp. 285-288, September 1978.
- [38]. Gans, W. L. and Nahman, N. S., "Continuous and Discrete Fourier Transform of Step-like Waveforms," *IEEE Transactions on Instrumentation and Measurement*, vol. IM-31, no. 1, pp. 97-101, June 1982.
- [39]. Nahman, N.S., "Introduction to Time Domain Measurements and Applications," Class Lecturer Notes (followed in EE 5016).
- [40]. Von Hippel, A. R., *Dielectric Materials and Applications*, Wiley, N. Y., 1961.
- [41]. Glasser, L. A., "An Analysis of Microwave De-embedding Errors," *IEEE Transactions on Microwave Theory and Techniques*, vol. MTT-26, no. 5, pp. 379-380, May 1978.
- [42]. Baker-Jarvis, J., Janezic, M. D., Grosvenor, Jr., J. H., and Geyer, R. G., "Transmission/Reflection and Short-Circuit Line Methods for Measuring Permittivity and Permeability," NIST Technical Note 1355-R, December, 1993.
- [43]. Whinnery, J. R., Jamieson, H. W. and Robbins, T. E., "Coaxial-Line Discontinuities," *Proceedings of the IRE*, pp. 695-709, November, 1944.

CURRICULUM VITAE

Mr. Raqibul Mostafa was born in Bangladesh in 1966. He received his B.S. degree in Electrical and Electronic Engineering from Bangladesh University of Engineering and Technology (BUET), Dhaka, Bangladesh in 1991. He worked as a lecturer in the department of Electrical and Electronic Engineering for one and a half year. In 1993, he started his graduate studies in Electrical Engineering at Virginia Polytechnic Institute and State University. He worked as a research assistant during his graduate program. His areas of interest include time domain techniques and signal processing.